Journal of the Korean Ceramic Society
Vol. 55, No. 4, pp. 307–324, 2018.

https://doi.org/10.4191/kcers.2018.55.4.07

Review

Conversion-Alloying Anode Materials for Na-ion Batteries: Recent Progress, Challenges, and Perspective for the Future

Joo-Hyung Kim and Do Kyung Kim†

Department of Materials Science and Engineering, Korea Advanced Institute of Science and Technology (KAIST), Daejeon 34141, Korea

(Received April 20, 2018; Revised June 7, 2018; Accepted June 8, 2018)

ABSTRACT

Rechargeable lithium-ion batteries (LIBs) have been rapidly expanding from IT based applications to uses in electric vehicles (EVs), smart grids, and energy storage systems (ESSs), all of which require low cost, high energy density and high power density. The increasing demand for LIBs has resulted in increasing price of the lithium source, which is a major obstacle to wider application. To date, the possible depletion of lithium resources has become relevant, giving rise to the interest in Na-ion batteries (NIBs) as promising alternatives to LIBs. A lot of transition metal compounds based on conversion-alloying reaction have been extensively investigated to meet the requirement for the anodes with high energy density and long life-time. In-depth understanding the electrochemical reaction mechanisms for the transition metal compounds makes it promising negative anode for NIBs and provides feasible strategy for low cost and large-scale energy storage system in the near future.

Key words : Na-ion battery, Anode, Nano-materials, Conversion reaction, Alloying reaction

1. Introduction

Rechargeable lithium-ion batteries (LIBs) were first introduced into the battery market by Sony and Asahi in 1991. Their production has seen massive growth led by Japanese companies such as Panasonic and Hitachi and centering on the information technology (IT) device industry.[1)] Since 2000, Korean companies such as LG Chemical, Samsung SDI, and Chinese manufacturers including ATL and BYD have entered the market. With the development of high capacity battery technologies, lithium ion batteries have become widely used in commercial industries mainly including smart phones, tablet PCs, laptops, and automobiles because of their high energy density and long life-time compared with the other types of rechargeable batteries.[2)] The motivation for using a lithium-based battery technology rather than that of a primary (non-rechargeable) battery such as alkaline, mercury, or zinc chloride, relied initially on the fact that Li is the most electropositive (−3.04 V versus standard hydrogen electrode; SHE) and lightest metal (equivalent weight M = 6.94 $g \cdot mol^{-1}$, and specific gravity r = 0.53 $g \cdot cm^{-3}$). The advantages of Li metal for batteries were first demonstrated in the 1970s with the assembly of primary Li cells.[3,4)] Owing to their high theoretical capacity and fast Li-ion mobility, Li-ion batteries rapidly found applications as power sources for IT based applications as well as implantable medical devices.

As the global market for lithium-ion secondary batteries is growing and expected to grow to several times the size of the present market in 10 years,[1,5)] soaring demand for lithium metal has meant that the global supply chain for lithium has had to grow nearly exponentially to keep up. The annual demand for lithium carbonate (Li_2CO_3) as a lithium metal has increased more than 3-fold compared with previous year in China.[6)] The present production of Li_2CO_3 is about half what would be needed to convert the 50 million cars produced every year into 'plug-in hybrid electric vehicles' (with an electric motor powered by a 7 kWh Li-ion battery and a combustion engine). However, the current LIBs rely on intercalation-based electrodes, that provide only limited practical energy density (~230 $Wh \cdot kg^{-1}$) in commercial electrical vehicles. Moreover, LIBs use non-aqueous, organic electrolytes that are prone to safety issues.[1,3)]

Sodium is one of the most naturally abundant elements and has low cost, low toxicity, and very suitable redox potential ($E^{o}_{(Na+/Na)}$ = −2.71 V versus standard hydrogen electrode; only 0.33 V positive of lithium). Sodium has physiochemical characteristics (iconicity, electronegativity, and electrochemical reactivity) similar to those of lithium. The ionic size of sodium ions is larger than that of lithium ions and Na has different bonding characteristics that have effects different from those of lithium systems. Most of the academic interest in Na-ion batteries has originated from the fact that similar materials (various crystal structures used in conventional Li-ion batteries) can be applied to Na-ion batteries.[7)] Na-ion batteries have gathered considerable interest in the field of large-scale energy storage systems (ESSs) because of the cost effectiveness and environmental

†Corresponding author : Do Kyung Kim
E-mail : dkkim@kaist.ac.kr
Tel : +82-42-350-4118 Fax : +82-42-350-3310

friendliness.[8-13] The early interest in sodium-based materials has been revisited on account of the natural abundance of sodium and relatively lower cost than of lithium resources. Therefore, rechargeable sodium-ion batteries (NIBs) can be considered for utilization in applications requiring lower cost and less weight/volume limitation in terms of the need to go beyond the limits of Li-ion batteries. Furthermore, from the perspective of articulation of Li and Na systems, there are no obstacles to research on Na-ion batteries because their binders, electrolytes, additives, etc., are similar. Inspired by these points, creation of an intercalative material applicable for Na-ion crystal structures has become attractive due to their potential for working well in sodium ion batteries. Recent attention to NIBs has led to many new designs for electrode materials being reported and proposed.[14,15]

In order to construct a high performance Na-ion full cell, extensive investigation of electrode materials for sodium ion batteries has to be carried out not only various transition metal oxides and phosphates as cathode materials, but also candidate anode materials.[16] Graphite has remained the most commonly used anode for Li-ion batteries since Sony and Asahi Kasei released the first commercial LIBs. However, the use of graphite results in poor electrochemical properties in sodium systems because sodium ions are nearly 25% larger than lithium ions.[17] The larger size makes it more difficult for sodium ions to be inserted into the graphene sheets. Hard carbon showed better electrochemical performance than conventional graphite anode in sodium systems with 0.3 V of average operating voltage and 250 $mAh \cdot g^{-1}$ of reversible discharge capacity.[18] However, its energy density is too low for it to be used as anodes for large-scale energy systems. Transition metals (e.g., Sn, Sb, Ge, Si, Pb) based on alloy reactions ensure considerable capacity as well as a relatively low redox potential because of their various oxidation states. Unfortunately, these types of materials undergo severe capacity fading due to the pulverization caused by large volume expansion during cycling.[16,19]

Several types of transition metal oxides (TMOs), transition metal chalcogenides (TM-Chs; TM-S, Se, Te), and transition metal phosphides (P) based on conversion reactions have been reported for use as anode materials for NIBs.[20] TMOs and TM-Chs, in particular, have advantages in terms of cost effectiveness, because they can be prepared easily via various synthesis processes (e.g., solid state reaction, high energy ball milling, spray pyrolysis, hydro/solvo-thermal synthesis, chemical vapor deposition, gas phase reaction, co-precipitation, electro-plating, electro-spinning, sulfurization, selenization). They also deliver high specific capacity comparable to transition metal-based electrodes. However, only a few TMOs in sodium-based systems have been able to utilize their high theoretical specific capacity because of their irreversibility for charge/discharge processes. The reaction mechanisms of both TMOs and transition metal chalcogenides (TM-Chs) are known to involve Na^+ insertion into host materials with subsequent formation of sodium chalcogenide (Na_xCh, $x \leq 2$) and sodium-transition metal alloys. At the beginning of the discharge process, the conversion reaction between TM-Chs and Na^+ is assumed to generate the transition metal and sodium chalcogenide (Na_xCh, $x \leq 2$). Successive reactions make up the alloying process, which transforms transition metals to sodium-transition metal alloys. These correspond to a conversion reaction and subsequent alloying reaction, respectively.

Moreover, the research on the anode materials for Na-ion batteries is still challenging. There remain problems that must be solved to improve the reversibility of sodium ion flow during electrochemical reactions. Selection of anode materials adequate for use in NIBs should provide low redox potential, high specific energy, good Na^+ kinetics, and cycling stability. The most common strategies used to meet these requirements are morphology design, the introduction (or modification) of carbonaceous material, and the optimization of cell components (e.g., electrolyte, binder, additives). Remarkable research in the field of TM-Ch has led to advances in terms of productivity, and to excellent electrochemical performance.

2. Alloy-type Anode Materials

Alloy-type anodes for NIBs have been extensively reported by a number of authors over the last few years.[19,21] Alloy anodes (Si, Ge, Sn, Pb, Sb, and P) have been attractive candidate materials for use in NIBs due to their high theoretical capacities as shown in Fig. 1(a). The general alloying reaction for electrochemical sodiation is shown in reaction (1).

$$\text{Alloy anodes (Si, Ge, Sn, Pb, Sb, or P)} + x\,Na^+ + x\,e^- \leftrightarrow Na_x\text{-TM alloys} \quad (1)$$

The alloying mechanism of each transition metal has been considerably studied using various methods by many groups. Komaba *et al.* examined the redox reaction of Sn-polyacrylate electrodes in aprotic Na cells with different types of binder, and then confirmed that Sn was transformed into a crystalline $Na_{15}Sn_4$ phase after full discharge using *ex situ* X-ray diffraction (XRD).[22] Huang *et al.* studied phase transformation, which is associated with volume expansion, during electrochemical sodiation using *in situ* transmission electron microscopy (TEM) as shown in Fig. 1(b). The microstructural change from Na_xSn ($x \sim 0.5$) to the final $Na_{15}Sn_4$ corresponded to (60 and 420) % volumetric expansion in accordance with the sodiation process. The final equilibrium phase for a Na-Sn alloy is $Na_{15}Sn_4$, which exhibits a high theoretical capacity (847 $mAh \cdot g^{-1}$) because of its high number of valence electrons.[23] Ceder *et al.* showed the sodiation voltage curves obtained from the density functional theory (DFT) total energies for the operating voltage of the group IVa elements Si (954 $mAh \cdot g^{-1}$), Ge (369 $mAh \cdot g^{-1}$), Sn (847 $mAh \cdot g^{-1}$), and Pb (485 $mAh \cdot g^{-1}$), and reported voltage profiles below 0.5 V.[19] Germanium has also

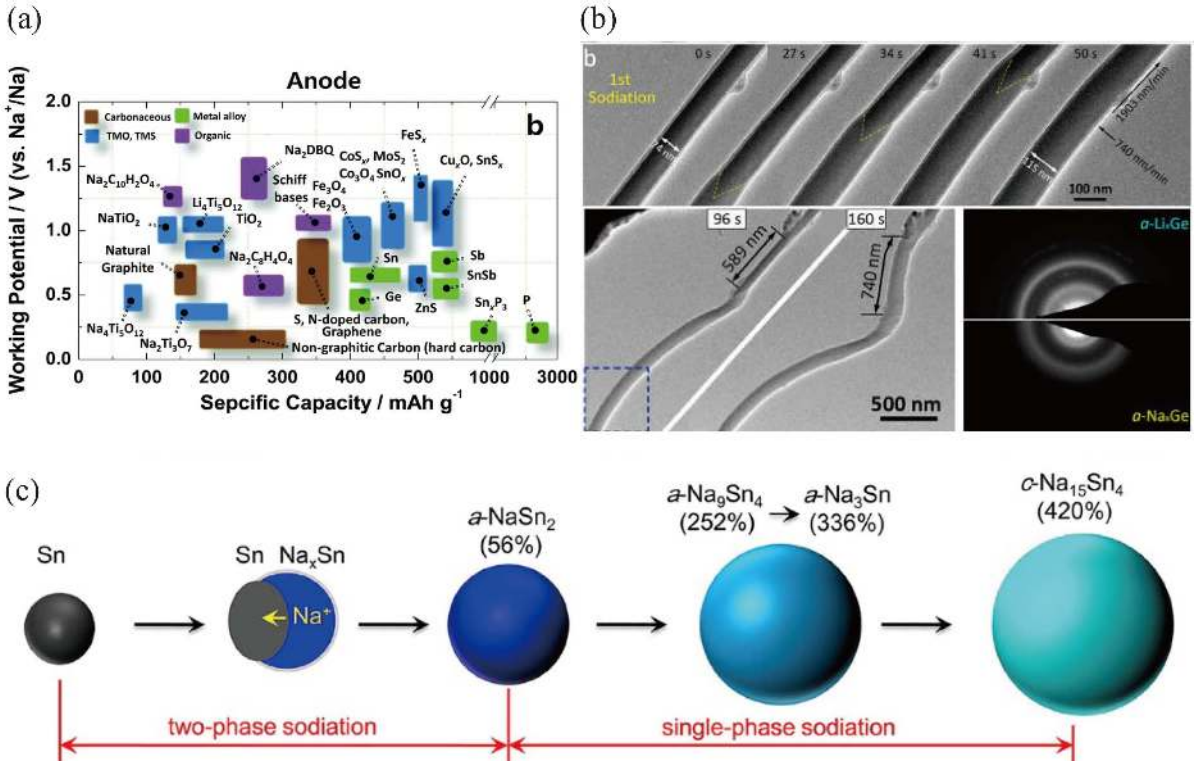

Fig. 1. (a) Recent research progress for andoe in sodium ion batteries. Reproduced and modified with permission from ref. 14. Copyright 2017 The Royal Society of Chemistry. (b) Time series images of sodiation of amorphous Ge nanowire and electron diffraction pattern. Reproduced and modified with permission from ref. 28. Copyright 2016 The American Chemical Society. (c) Schematic illustration of the structural evolution of Sn nanoparticles during the sodiation. Reproduced and modified with permission from ref. 29. Copyright 2012 The American Chemical Society.

been extensively studied as a negative electrode material for LIBs because of its high lithium storage capacity until the electrode crystallizes into $Li_{15}Ge_4$ (1384 $mAh \cdot g^{-1}$) and its high lithium diffusivity.[24,25] The dissimilarity between Li and Na ions results in several orders of magnitude slower sodium diffusion than that of lithium in germanium. When sodium ions diffuse to interstitial sites in a germanium lattice, the larger radius of sodium (relative to lithium) requires much higher activation energy for hopping (0.51 eV for lithium, 1.5 eV for sodium). Loic *et al.* first reported the electrochemical properties of germanium thin-film electrodes during Na-ion electrochemical reaction. To investigate sluggish Na diffusivity into the interstitial sites in the lattice, the reaction potential data obtained with constant current and quasi-equilibrium measurements using the galvanostatic intermittent titration technique (GITT) are discussed and compared to X-ray absorption spectra (XAS) results.[26,27]

In spite of their high theoretical capacity, more study of transition metals is required to reduce large volume expansion (which results in pulverization) by transformation to Na-TM (Si, Ge, Sn, Pb, Sb, and P) alloys. Especially, the volume expansion of Na-Sn alloys is about five times with respect to initial volume of tin as shown in Fig. 1(c). It has been reported that the deterioration of material properties and shortened cycle life due to pulverization are serious problem in long-time cycling tests.[24,28,29] It causes a condition in which the electrode material and current collector separate from each other, which is associated with fatal fading of capacity. To solve this problem, a variety of studies are being conducted. These include such as physically preventing volume expansion using a carbon matrix,[30,31] or minimizing the strain-stress that accompanies volume expansion using nano-sizing.[32,33] Recently, there has been much research involving such as Na-TM alloys and matrix composites to reduce pulverization of transition metals. However, so far, no one has demonstrated perfect suppression of the volume expansion of transition metal during sodiation and de-sodiation, with reversible theoretical capacity.

3. Conversion-alloying Anode Materials

3.1. Transition metal oxides

Transition metal oxides can react with Na^+ through a sequential conversion-alloying reaction. The conversion reaction between metal oxide and sodium takes place during the first discharge, generating sodium oxide and transition metal as shown in reaction (2). If the alloy anodes (Si, Ge, Sn, Pb, Sb, and P) remaining after the conversion reaction can be alloyed with sodium ions, they form a transition metal-sodium alloy as in reaction (3).

Conversion reaction: $TM\text{-}O_x + 2x\ Na^+ + 2x\ e^- \leftrightarrow TM + x\ Na_2O$ (2)

Alloying reaction: $TM + y\ Na^+ + y\ e^- \leftrightarrow Na_y\text{-}TM\ alloy$ (3)

The remaining sodium oxide does not participate in successive cycles if the sodium oxide cannot secure the reversibility of Na diffusion. Problems with metal oxides have been pointed out, and these include such as the intrinsic irreversibility of the material and volume expansion (similar to alloy-based materials), which accompanies severe capacity fading during sodiation.

3.1.1. Tin oxide

Various transition metal materials can achieve high capacity by an alloying reaction with sodium ions. For example, Sn reacts with 3.75 sodium atoms to provide a capacity of 1047 $mAh{\cdot}g^{-1}$, which is the highest among all the alloy anodes (except phosphorus). However, these transition metal materials exhibit a high volume expansion (4.2 times or more) of conventional Sn during the alloying reaction with sodium. This causes not only physical binding between the electrode material and the current collector, but also causes high strain-stress inside the material during charge/discharge reactions. As a result, it has been reported that the characteristic deterioration of life time due to pulverization remains a serious problem in long-term cycling tests. To solve this problem, a variety of studies are being conducted that include such as physically preventing volume expansion using a carbon matrix or minimizing strain-stress due to volume expansion using nano-sizing. Transition metal oxide-carbon composites have been reported as the common method to relieve volume expansion during the cycling, but also reduce the specific capacity because of the unnecessary carbon content. To try to overcome this shortcoming, Wang *et al.* reported the size of SnO_2 nanoparticles plays a critical role in electrode performance as shown in Fig. 2(a).[34] SnO_2 nanoparticles (~ 5 nm) anchored on an rGO framework offers a buffering space and delivers high specific capacity (480 $mAh{\cdot}g^{-1}$ at 50 $mA{\cdot}g^{-1}$; 0.1 C-rate) and good rate capability (125 $mAh{\cdot}g^{-1}$ at 1000 $mA{\cdot}g^{-1}$; 2 C-rate).

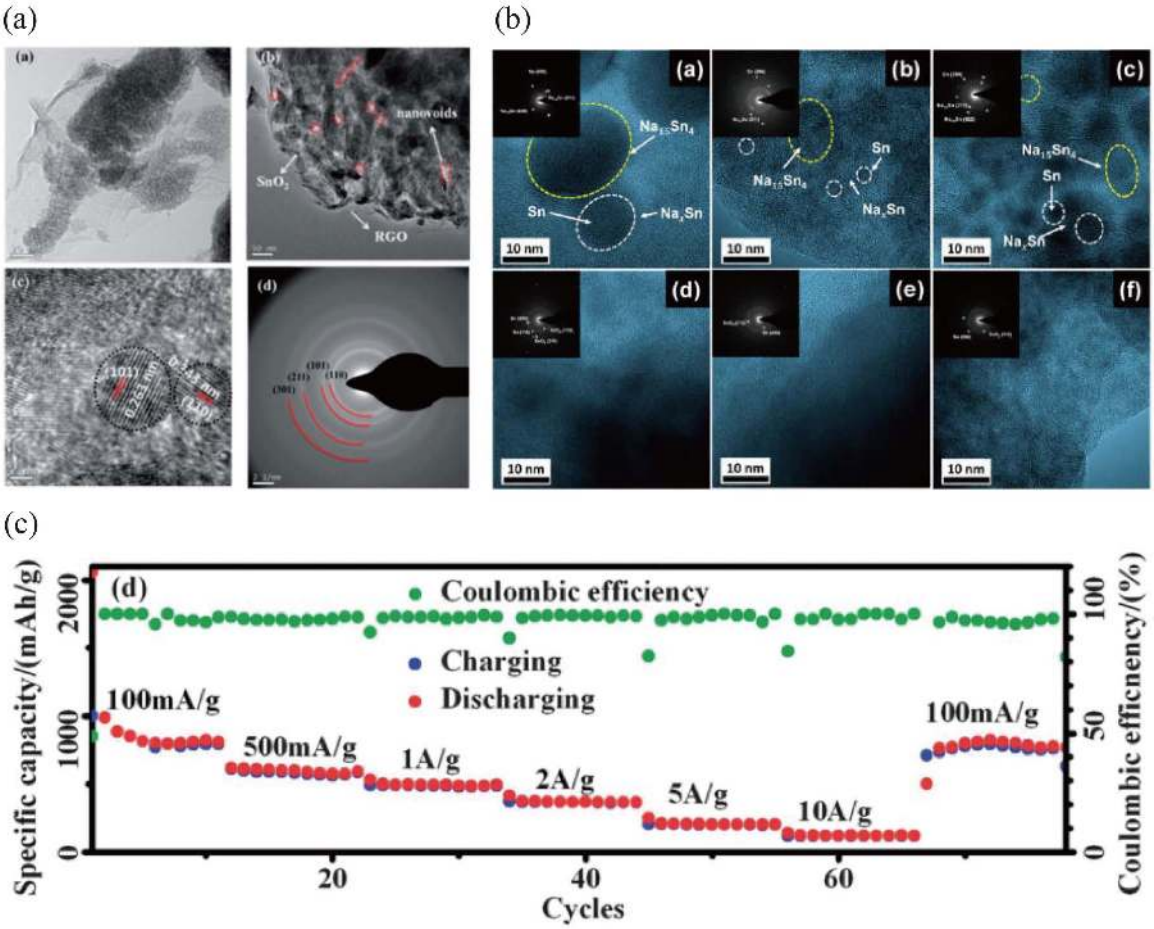

Fig. 2. (a) Schematic illustration of sodium storage after discharge process of the SnO_2-rGO nanocomposite anode. Reproduced and modified with permission from ref. 34. Copyright 2014 The Royal Society of Chemistry. (b) HR-TEM images of SnO_2/C electrodes during first cycling. (Insets: SAED patterns for corresponding TEM images). Reproduced and modified with permission from ref. 37. Copyright 2015 The American Chemical Society. (c) Rate performance for the composite electrode discharging at various rates from 100 $mA{\cdot}g^{-1}$ to 10 A g^{-1}. Reproduced and modified with permission from ref. 35. Copyright 2013 The Royal Society of Chemistry.

Fig. 2(c) shows that Song *et al.* aimed to form a complex between SnO_2 and graphene prepared using facile hydrothermal synthesis.[35] Tin dioxide can be well distributed on graphene oxide sheets when aided by dispersive hydrophilic radicals. This nanostructured composite exhibits not only better cycle performance but also better rate performance, with a long lifespan (> 1000 cycles). Patra *et al.* synthesized 1 nm SnO_2 particles uniformly dispersed and tightly connected to carbon supports.[36] This arrangement provided an initial charge-capacity of 400 $mAh \cdot g^{-1}$ at 100 $mA \cdot g^{-1}$ and capacity-retention of 82% after 100 cycles. The lower than theoretical capacity of the 1 nm SnO_2 nanoparticle electrode can be explained by an incomplete alloying reaction because of the lower diffusivity of Na in Sn. In addition, in a number of studies there are reports of introducing carbon supports such as carbon additives, carbon nanotubes, and graphene nanosheets to solve the low intrinsic electron conductivity problem of SnO_2; however, none could approach the theoretical capacity in Fig. 2(b).[37-40] Xie *et al.* reported the fabrication of cross-linked 3-D conductive graphene networks with hierarchical pores and SnO_2 nanoparticles. This functional structure provides an efficient electron pathway within the graphene networks, but shows lower reversible capacity (< 400 $mAh \cdot g^{-1}$) because of the high carbon content in the electrode material.[38] Huang *et al.* also reported a 3-D porous carbon encapsulated SnO_2 nanocomposite synthesized using an *in situ* methodology that delivered a reversible specific capacity of 280.1 $mAh \cdot g^{-1}$ after 250 cycles at a current density of 100 $mA \cdot g^{-1}$.[39] Although it exhibited 100 $mAh \cdot g^{-1}$ after 100 cycles at a high current density of 1600 $mA \cdot g^{-1}$, the reversible capacity did not reach the theoretical capacity, as in other publications about the use of SnO_2 nanocomposite electrodes for NIBs.

3.1.2. Antimony oxide

Antimony (Sb) reacts with three sodium ions and has a theoretical capacity of 660 $mAh \cdot g^{-1}$, which is relatively smaller than that of tin (847 $mAh \cdot g^{-1}$). However, the process of sodiation and de-sodiation of antimony (Sb) can lead to longer lifetimes during long-term cycling tests than that of tin (Sn) because of the lower volume expansion (~ 3 times) during the alloying reaction than that of tin (4.2 times).[41] To date, tin oxides (SnO and SnO_2) has been extensively studied for the purpose of improving lifetimes by suppressing the volume expansion accompanying the charge/discharge reactions of Sn with Na. As the same strategy, a variety of research has been conducted to increase the reversible specific capacity of antimony oxides (Sb_2O_3 and Sb_2O_5). Anti-

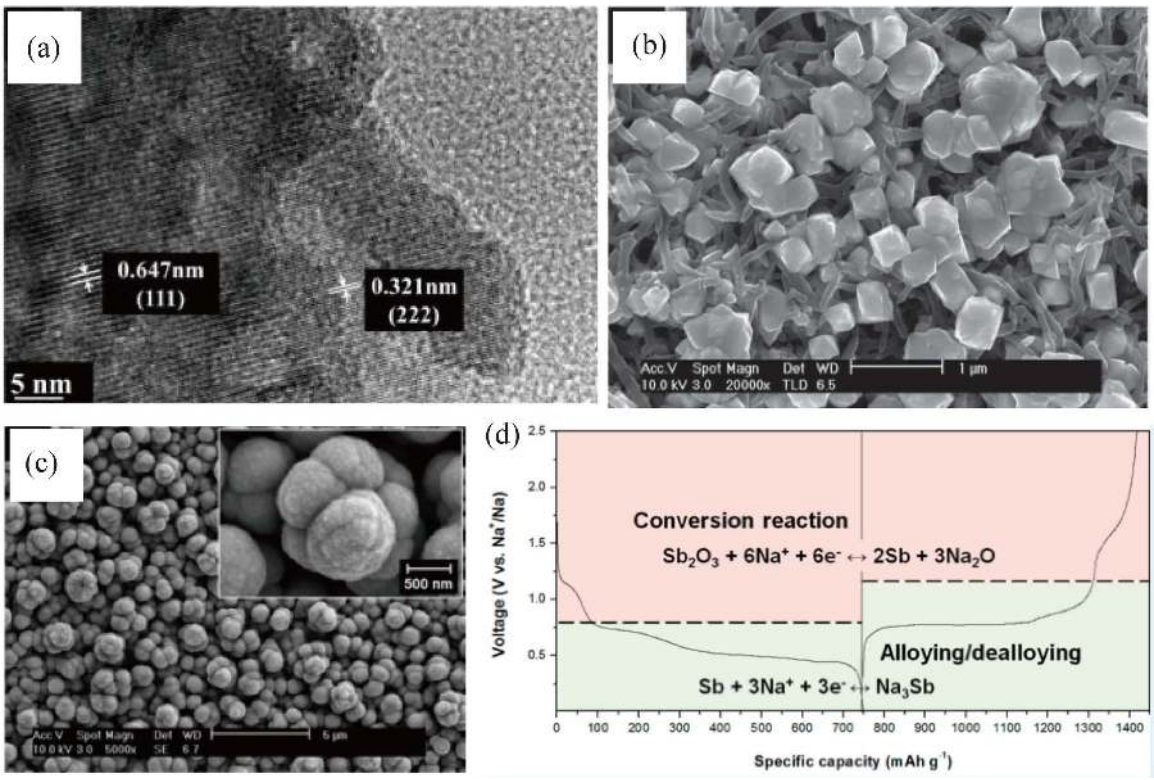

Fig. 3. (a) High resolution TEM image of synthesized Sb_2O_3 film. Reproduced and modified with permission from ref. 46. Copyright 2014 The American Chemical Society. (b) SEM image of the Sb/Sb_2O_3 nanodeposits electrodeposited on the polypyrrole nanowires. Reproduced and modified with permission from ref. 42. Copyright 2015 WILEY-VCH Verlag GmbH & Co. KGaA, Weinheim. (c) SEM images of Sb/Sb_2O_3 composites prepared by galvanostatic electrodeposition. Reproduced and modified with permission from ref. 43. Copyright 2015 The American Chemical Society. (d) Electrochemical reaction mechanism of Sb/Sb_2O_3 composites. Reproduced and modified with permission from ref. 43. Copyright 2015 The American Chemical Society.

mony oxides (Sb_2O_3 and Sb_2O_5) react with 10 and 14 sodium ions per mole, respectively, thus exhibiting a theoretical specific capacity of about (919 and 1236) $mAh \cdot g^{-1}$.

Hu *et al.* reported combined conversion-alloying electrochemical reactions of Sb_2O_3, delivering a reversible charge capacity of 509 $mAh \cdot g^{-1}$ at a current density of 0.05 $A \cdot g^{-1}$, and retains as high as 265 $mAh \cdot g^{-1}$ at an ultrahigh current density of 5 $A \cdot g^{-1}$ as shown in Fig. 3(a). Porous 3-D Sb-Sb_2O_3-Polypyrrole (PPy) nanocomposites were fabricated using a facile electrodeposition method with a PPy nanowire network as shown in Fig. 3(b).[42] They exhibited a reversible charge capacity of 512.01 $mAh \cdot g^{-1}$ over 100 cycles, and outstanding rate capability (299 $mAh \cdot g^{-1}$ at 3300 $mA \cdot g^{-1}$, 56.7% of the charge capacity). Although the Sb-Sb_2O_3-PPy electrode exhibited excellent electrochemical properties, the reversible capacity was lower than the theoretical value of a metallic Sb electrode due to its carbon content (~ 15%). Fig. 3(c) shows that Sb-Sb_2O_3 composites using a one-step electrodeposition process in an aqueous electrolytic bath.[43] The morula-like Sb-Sb_2O_3 composites delivered a reversible capacity of 670 $mAh \cdot g^{-1}$, which is beyond the theoretical capacity of Sb (660 $mAh \cdot g^{-1}$). These composites were of metallic Sb and crystalline Sb_2O_3 in a molar ratio of 9 : 1. The high specific capacity resulted from the reversible formation of Na_2O and Sb_2O_3 that occurs in addition to the alloying reaction of Sb with Na as shown in Fig. 3(d). In many of the studies in the literature graphene oxide was introduced to find appropriate agreement between the capacity increase of antimony oxide and the improvement of the rate characteristics. Wang *et al.* synthesized a Sb_2O_4-reduced graphene oxide (rGO) via solvothermal synthesis with different graphene oxide content in the nanocomposite.[44] The Sb_2O_4-rGO nanocomposite containing 18 wt% of graphene oxide showed a rechargeable capacity of 551 $mAh \cdot g^{-1}$ after 100 cycles and a rate performance of 401 $mAh \cdot g^{-1}$ at a current density of 1 $A \cdot g^{-1}$. However, there was still an obstacle to its use in development of high-performance NIB anodes because of the intrinsic properties of the antimony oxide-based materials. Fei *et al.* reported a flexible Sb_2O_3-carbon cloth (CC) composite used as a free-standing anode, which was fabricated using a simple solvothermal method.[45] This electrode delivered 900 $mAh \cdot g^{-1}$, which is very close to the theoretical capacity of antimony oxide (Sb_2O_3), after 100 cycles at a low current density of 50 $mA \cdot g^{-1}$. The outstanding electrochemical performance was attributed to the homogeneous growth of Sb_2O_3 nanoparticles on the CC, which improved electronic migration, sodium ion diffusion, and structural stability during the conversion and alloying reactions.

3.1.3. The other transition metal oxides

A number of candidate anode materials based on a sodium insertion host for SIBs have been intensively studied due to their low cost, nontoxicity, low operation voltage, low strain, and excellent cyclability.[19,21] Generally, titanium-based materials deliver low specific capacity due to the limitation of alkali-ion storage sites. Spinel $Li_4Ti_5O_{12}$ is one of the most attractive materials for a so called "zero-strain" anode for LIBs. It was first reported and further studied as an anode for NIBs by Zhao and Sun.[47,48] The $Li_4Ti_5O_{12}$ electrode can also store sodium with an average voltage of 0.91 V, delivering a reversible capacity of 155 $mAh \cdot g^{-1}$, and offers the best stable cyclability. A three-phase separation mechanism ($2Li_4Ti_5O_{12} + 6Na^+ + 6e^- \leftrightarrow 2Li_7Ti_5O_{12} + Na_6LiTi_5O_{12}$) of the electrode, with respect to sodium diffusion, can be predicted by density functional theory (DFT) calculations, which results have been confirmed through *in situ* synchrotron XRD and advanced TEM techniques. Tarascon and Palacin's group first ever reported that $Na_2Ti_3O_7$ reversibly reacted with sodium as a low average potential of 0.3 V (demonstrating 200 $mAh \cdot g^{-1}$) to reversibly uptake two Na ions per formula unit.[49] P2-type layered $Na_{0.68}[Li_{0.22}Ti_{0.78}]O_2$ delivered a reversible specific capacity of 116 $mAh \cdot g^{-1}$ (corresponding to 0.38 Na^+ ion insertion per formula unit) at an average storage potential of 0.75 V. It showed an ultra-long cycle life with 75% capacity retention, and confirmed that the volume change during Na^+ insertion/extraction was only 0.77% (zero strain) after 1200 cycles.[50] Recent progress on Ti-based sodium insertion electrodes has provided opportunities for the development of large-scale stationary energy storage systems.[51] Most of the intercalative materials based on sodium titanates such as $Na_2Ti_3O_7$, $Na_2Ti_6O_{13}$,[52] $Na_{0.68}[Li_{0.22}Ti_{0.78}]O_2$, and sodium nonatitanate[53] have been investigated for creation of stable anode materials with low operating voltages, but their practical capacity did not meet expectations for the energy storage applications of the future.

Recently, many metal oxides and sulfides have been studied as materials for negative electrodes for NIBs since the transition metal oxide spinel $NiCo_2O_4$ was first reported as an anode for NIBs in 2002.[54] $NiCo_2O_4$ undergoes a phase transformation to metallic Co and Ni after full sodiation, which was demonstrated by *ex situ* XRD. $NiCo_2O_4$ delivered a reversible capacity of 200 $mAh \cdot g^{-1}$, which was much lower than its theoretical capacity (890 $mAh \cdot g^{-1}$). This is the first time that a reversible conversion reaction was found for the mixed spinel composite, thereby providing an alternative anode material and a new approach for Na-ion batteries. Inspired by this electrode material, there have been studies reporting various combinations of metal oxides and sulfide as anodes for NIBs.[55-62] Iron oxides (Fe_2O_3 and Fe_3O_4) are attractive anodes due to their high theoretical capacity, easy synthesis, low toxicity, and low cost.[56,57,60] Nano-crystallized Fe_3O_4 (10 nm) prepared by the precipitation method, had a demonstrated reversible capacity of 160 - 170 $mAh \cdot g^{-1}$ with excellent capacity retention. The particle size of Fe_3O_4 has an effect on its structural change and electrochemical activity, which was confirmed by *ex situ* XRD for the cycled electrode samples.[56] In terms of cost effectiveness, Fe_3O_4 is one of the most promising potential anode materials for sodium-ion battery systems. A full NIB cell based on $Na[Ni_{0.25}Fe_{0.50}Mn_{0.25}]O_2$-$Fe_3O_4$/C with an electrolyte (NaC-

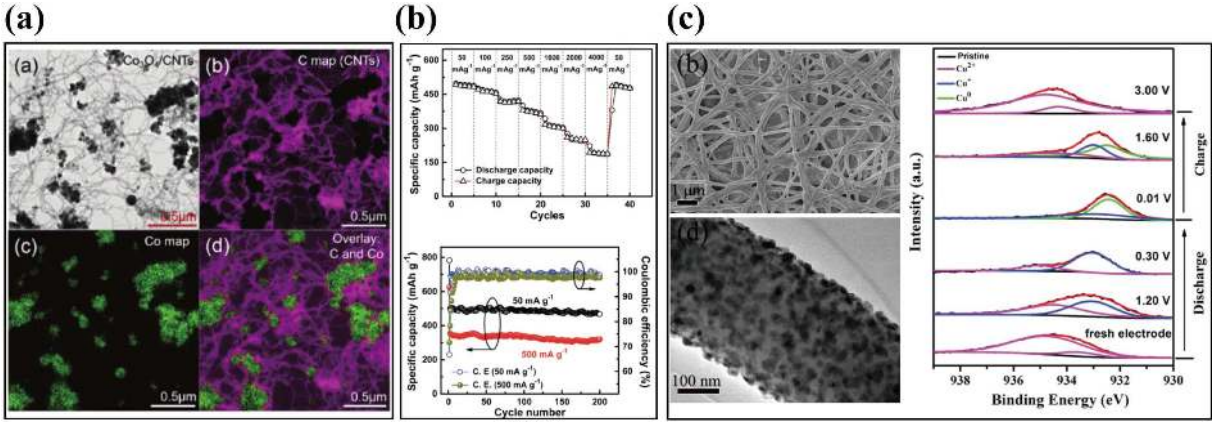

Fig. 4. (a) Elemental distributions of the Co_3O_4/CNT compostie. Reproduced and modified with permission from ref. 61. Copyright 2015 The Royal Society of Chemistry. (b) Electrochemical performance of the NTO-powder-based electrode. Reproduced and modified with permission from ref. 55. Copyright 2016 The Royal Society of Chemistry. (c) Microstructures and Ex situ XPS spectra of CuO@C nanocomposite. Reproduced and modified with permission from ref. 62. Copyright 2016 WILEY-VCH Verlag GmbH & Co. KGaA, Weinheim.

lO_4 in EMS/FEC) was investigated, and delivered a reversible capacity of 130 mAh·g^{-1} and 76.1% capacity retention after 150 cycles.[63] Similarly, Kuma *et al.* reported the synthesis of pure Fe_3O_4 nanoparticles via the hydrothermal method, and investigated their electrochemical performance with different binder systems (PVDF and Na-alginate).[57] Fe_3O_4 nanoparticles with the alginate binder delivered stable capacity of 248 mAh·g^{-1} at 0.1 C-rate after 50 cycles. The Na-ion full cells in which a Fe_3O_4-alginate anode and $Na_3V_2(PO_4)_3$-graphene cathode were combined, confirmed the potential to apply these directly to realize low-cost NIBs in the future. Many anodes of these types have been studied extensively, including CoO, CuO, NiO, MnO_2, and MoO_3 for Na-ion battery systems as shown in Fig. 4.[55,58,59,61,62] The electrochemical performances of transition metal oxide as an anode for sodium-ion batteries are summarized in Table 1.

Table 1. Summary of Transition Metal Oxide Anodes for Sodium-Ion Batteries

TM-O	Initial charge capacity [mAh·g^{-1}]	Current density [mA·g^{-1}]	Cycle number	Capacity retention	Carbon/GO Content in the anode [%]	Reference
SnO_2/rGO	800	100	200	90	38	ref. 35
SnO_2/rGO	407	100	150	81.3	36	ref. 34
SnO_2/C	433	152	200	95.3	23	ref. 37
SnO_2/Graphene	451	20	100	71.4	61.5	ref. 38
SnO_2/C	305.7	100	250	91.6	25.5	ref. 39
SnO_2/rGO	400	20	100	82	20	ref. 36
SnO_2/N-doped graphene	518.5	50	50	57.9	37	ref. 40
Sb_2O_3	550	50	200	75	0	ref. 46
Sb_2O_3	657	66	100	91.8	0	ref. 43
Sb/Sb_2O_3	565	660	180	92.8	0	ref. 64
Sb/Sb_2O_3/C	527	66	100	98.3	15	ref. 42
Sb_2O_3/rGO	503	100	50	> 100	Unmentioned	ref. 65
$NiCo_2O_4$	~ 300	89	4	83	0	ref. 54
Fe_2O_3	~ 190	20	30	88	0	ref. 56
Fe_2O_3	250	83	50	98	0	ref. 57
Fe_2O_3/N-doped graphene	401	50	50	76	Unmentioned	ref. 60
Co_3O_4	~ 600	89	50	~ 80	0	ref. 59
Co_3O_4/CNT	420	50	100	96	~ 10	ref. 61
CuO/CNF	528	100	100	83	46	ref. 62
CuO/rGO	503	100	50	92.8	27.3	ref. 58

3.1.4. Limitation of transition metal oxide anodes

Transition metal oxide can be expected to have high specific capacity as anode materials for sodium ion batteries due to their variety of oxidation states, but they have poor rate performance owing to the extremely low intrinsic electrical conductivity of the electrode. Moreover, the sluggish diffusivity of sodium ions in the transition metal oxides limits the rate of sodium insertion/extraction (low energy density), and the low surface area of the bulk electrodes restrains their capacitive contribution (low power density). To solve these problems, many studies have been carried out to improve the electrical conductivity by introducing a carbon matrix and composite, and making short diffusion paths by limiting the particle size to nanometer-scale to enhance the ionic conductivity. However, these noteworthy attempts were insufficient to realize the necessary performance of sodium for high-efficiency energy storage. If a carbon material is applied to overcome the intrinsic properties of the transition metal oxides, the weight ratio of the oxides is remarkably decreased as the fraction of carbon matrix in the electrode material is increased. Furthermore, various problems are encountered in the packaging process as well as the practical capacity in actual battery applications. The rational design of controllable microstructure and electron conductive components of transition metal oxides for high-performance NIB anode materials is both necessary and urgent.

3.2. Transition metal chalcogenides

Transition metal chalcogenides are chemical compounds consisting of at least one chalcogen anion and at least one more transition metal cation. Transition metal chalcogenides have attracted a great deal of interest as potential anode materials for NIBs because of their unique crystal structure, which consists of 2-D or quasi 2-D stacked layers like graphene nanosheets.[66,67] They guarantee a certain revers-

Table 2. Summary of Transition metal Chalcogenide Anodes for Sodium-Ion Batteries

TM-S	Initial charge capacity [mAh·g^{-1}]	Current density [mA·g^{-1}]	Cycle number	Capacity retention [%]	Carbon/GO Content in the anode [%]	Reference
Sn-SnS-C	416	100	150	87	20	ref. 68
SnS-C	548	100	80	97	20	ref. 69
SnS/rGO	1037	30	50	91	13.8	ref. 70
SnS_2/rGO	628	200	100	99	Unmentioned	ref. 71
SnS_2/rGO	590	200	300	86	19	ref. 72
SnS_2/rGO	$843_{(\text{only SnS})}$	100	100	98	29.2	ref. 73
Sn-S/rGO	956 / 852	50 / 100	50 / 100	94 / 87	12.9	ref. 74
SnSe/C	~ 600	143	50	> 100	~ 30	ref. 75
SnSe/C	447.7	500	200	72.5	~ 30	ref. 76
$SnSe_2$/rGO	660	100	100	78	24.4	ref. 77
SeTe	542.5	100	30	22	0	ref. 78
Sb_2S_3	707	50	50	> 100	0	ref. 79
Sb_2S_3	647	50	100	79	0	ref. 80
Sb_2S_3	~ 800	100	100	~ 70	10.5	ref. 81
MWCNTs/Sb_2S_3/PPy	596	50	80	82	41	ref. 82
Sb_2S_3/Graphite	661	1000	100	99.1	20	ref. 83
Sb_2S_3/rGO	670	50	50	> 95	17	ref. 84
Sb_2S_3/S-doped graphene	~ 710	500	200	96.7	7.82	ref. 85
Sb_2Se_3	360	100	50	80.3	0	ref. 86
Sb_2Se_3/C	657.6	200	100	73.8	~ 8	ref. 87
Sb_2Te_3/C	555	50	50	67	40	ref. 88
MoS_2	~ 700	67	50	> 85	0	ref. 89
MoS_2/CNF	~ 800	1000	100	> 60	38	ref. 90
$MoSe_2$/N,P-doped CNS	~ 430	500	1000	87	15	ref. 91
Co-doped FeS_2	~ 420	1000	400	~ 62	0	ref. 92
FeS_2@$FeSe_2$	348.8	1000	2700	~ 100	0	ref. 93
CoS_2/N,S-doped CNS	~ 680	1000	200	87	51	ref. 94
$CoSe_2$	595	500	40	91	0	ref. 95
GeS_2/rGO	805	100	100	89.4	30.3	ref. 96

ibility and conductivity because of their lower bonding energy. This difference in their discharge/charge characteristics can be attributed to the relative reversibility of the formation of sodium chalcogenides (Na_xCh; Ch = S, Se, and Te) compared to the formation of sodium oxides (Na_xO). The chalcogenide anion of the electrode material is converted to sodium polysulfide (Na_2Ch_x; $2 \le x \le 8$) during the conversion reaction, ultimately becoming sodium chalcogenide (Na_2Ch). This conversion reaction applies equally to other chalcogen ions. After the conversion reaction, the remaining the transition metal can be alloyed with sodium ions like the reaction (3) if the transition metal is the alloy anodes (Si, Ge, Sn, Pb, Sb, and P). They form a transition metal-sodium alloy as in reaction (5). The platform reaction can be expressed as indicated in reaction (4) and (5) below.

$$\text{Conversion reaction: TM-Ch}_x + 2x\ Na^+ + 2x\ e^- \leftrightarrow \text{TM} + x\ Na_2Ch \quad (4)$$

$$\text{Alloying reaction: TM} + y\ Na^+ + y\ e^- \leftrightarrow Na_y\text{-TM alloy} \quad (5)$$

Transition metal chalcogenides are considered strong candidates due to their unique physical properties. These include such as a tunable stoichiometric compositions, unique crystal structures, chemical properties such as rich redox sites, and relatively higher electrical conductivity, relative to their transition metal-oxide counterparts.[97-99] The electrochemical performances of transition metal chalcogenide as an anode for sodium-ion batteries are summarized in Table 2.

3.2.1. Tin chalcogenides

Tin chalcogenides (SnChs) have been used in lithium ion batteries (LIBs) as promising anode materials. Because 1 mole of SnCh or $SnCh_2$ could accommodate (5.75 or 7.75) moles of alkali ion$^+$, they were able to deliver high theoretical capacity (1022 or 1136) mAh·g^{-1}. The previous reports of tin sulfides as anode material for NIBs were only focused on improvement of battery performance by optimizing the electrode additives, using suitable electrolytes, and adjusting the content of graphene oxide.[70,71] Understanding of the reaction mechanism during sodiation/de-sodiation is still lacking, which leads to incomplete electrochemical utilization for Na-storage systems due to irreversibility of unfavorable conversion-alloying reactions.

Zhou *et al.* studied the structural changes of a hybrid SnS@graphene architecture via hydrothermal synthesis during cycling.[70] The electrode composite underwent fewer phase transitions after the conversion reaction than did SnS_2@graphene hybrid material, as revealed by *ex situ* XRD. This material can provide high reversible capacity and superior high-rate capability allowing the introduction of inexpensive and versatile synthesis techniques. Kim *et al.* prepared mixed Sn-S nanocomposites uniformly distributed on reduced graphene oxide via facile hydrothermal synthesis and a unique carbo-thermal reduction process as shown in Fig. 5(a). The product was ultrafine nanoparticles with crystalline size of 2 nm.[74] These nanocomposites have been experimentally confirmed to overcome the intrinsic drawbacks of tin sulfides such as large volume change (4.2 times), with accompanying cycle instability due to the pulverization problem, and sluggish diffusion kinetics. The mixed Sn-S ultrafine nanoparticles exhibit outstanding electrochemical performance: an excellent specific capacity of 1230 mAh·g^{-1} and an impressive rate capability (445

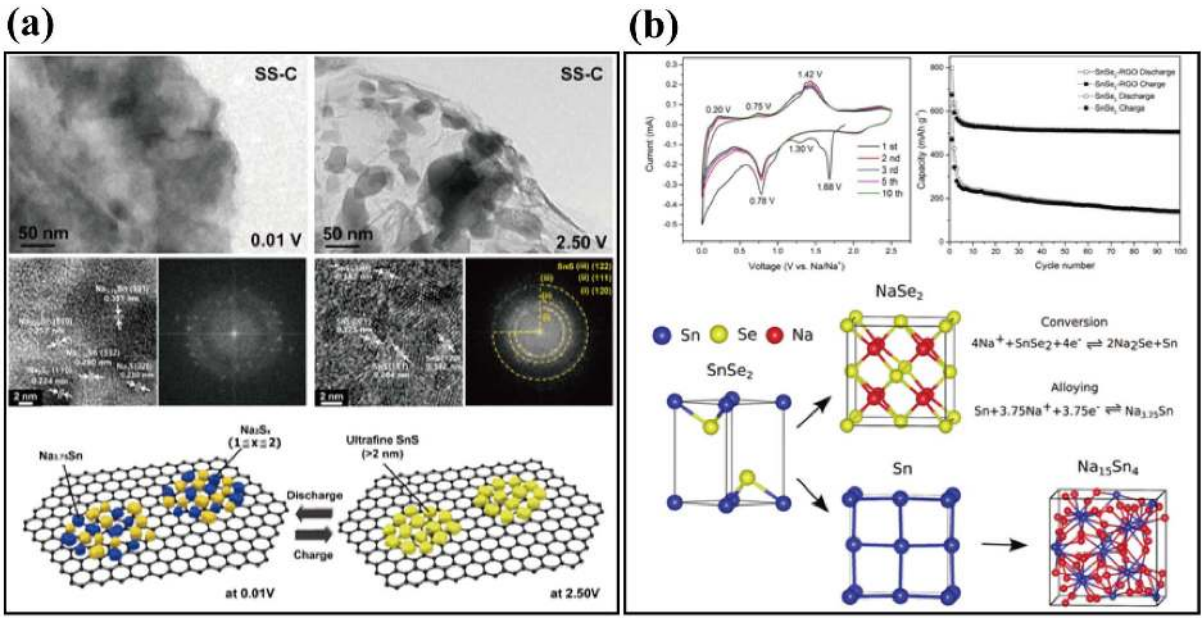

Fig. 5. (a) Ex situ images and schematic illustration of the mixed Sn-S/rGO nanocomposite. Reproduced and modified with permission from ref. 74. Copyright 2017 WILEY-VCH Verlag GmbH & Co. KGaA, Weinheim. (b) Electrochemical performances and schematic illustration of the structure evolution of $SnSe_2$ during the sodiation process. Reproduced and modified with permission from ref. 77. Copyright 2016 WILEY-VCH Verlag GmbH & Co. KGaA, Weinheim.

$mAh \cdot g^{-1}$ at 5000 $mA \cdot g^{-1}$). The electrochemical behavior of a sequential conversion-alloying reaction for the anode materials was investigated, revealing both the structural transition and the chemical state during the discharge/charge process. Kim *et al.* first examined SnSe-C composite, prepared via facile ball milling in Ar gas.[75] The reversible capacity of the composite was 707 $mAh \cdot g^{-1}$, delivering 91% of the theoretical capacity of SnSe (780 $mAh \cdot g^{-1}$). This calculation was based on the weight of SnSe alloy in the composite. The reversible sodiation/de-sodiation mechanism of SnSe was determined through *ex situ* XRD and TEM, which contributed to the development of transition metal selenide materials as anode materials for NIBs. Other tin selenide materials such as 2-D $SnSe_2$ alloy with rGO, were synthesized by a hydrothermal method in Fig. 5(b).[77] The $SnSe_2$-rGO nanocomposites delivered a reversible specific capacity of 515 $mAh \cdot g^{-1}$ at 0.1 $A \cdot g^{-1}$ after 100 cycles. The rGO is believed to stabilize the electrode, improve electron conductivity, and better tolerate volumetric changes during the sodiation/de-sodiation processes. Park *et al.* reported a difference in the electrochemical properties of cubic crystal-structured SnTe for Li and Na-ion battery anodes.[78] The electrochemically induced phase transition mechanism of SnTe electrodes during Li and Na insertion/extraction was investigated using various *ex situ* analysis techniques. SnTe was converted to $Li_{4.25}Sn$ and Li_2Te during lithiation; however, during Na insertion, SnTe experienced a quasi-intercalation reaction to Na_xSnTe ($x \leq 1.5$) and conversion to $Na_{3.75}Sn$ and Na_2Te.

3.2.2. Antimony chalcogenides

The electrochemical reaction mechanism in the sodiation/de-sodiation process of antimony chalcogenides has a conversion and alloying reaction principle similar to that of the tin chalcogenides. Zhu *et al.* prepared a flower-like Sb_2S_3 composite via a polyol reflux process that delivered reversible capacity of 835.3 $mAh \cdot g^{-1}$ (50 $mA \cdot g^{-1}$ after 50 cycles), near the theoretical capacity (946 $mAh \cdot g^{-1}$) of Sb_2S_3.[79] They insisted that such an improvement of the electrochemical performance was attributable to the unique flower-like structure of Sb_2S_3. This composite not only exhibited mitigated volume expansion, but also provided

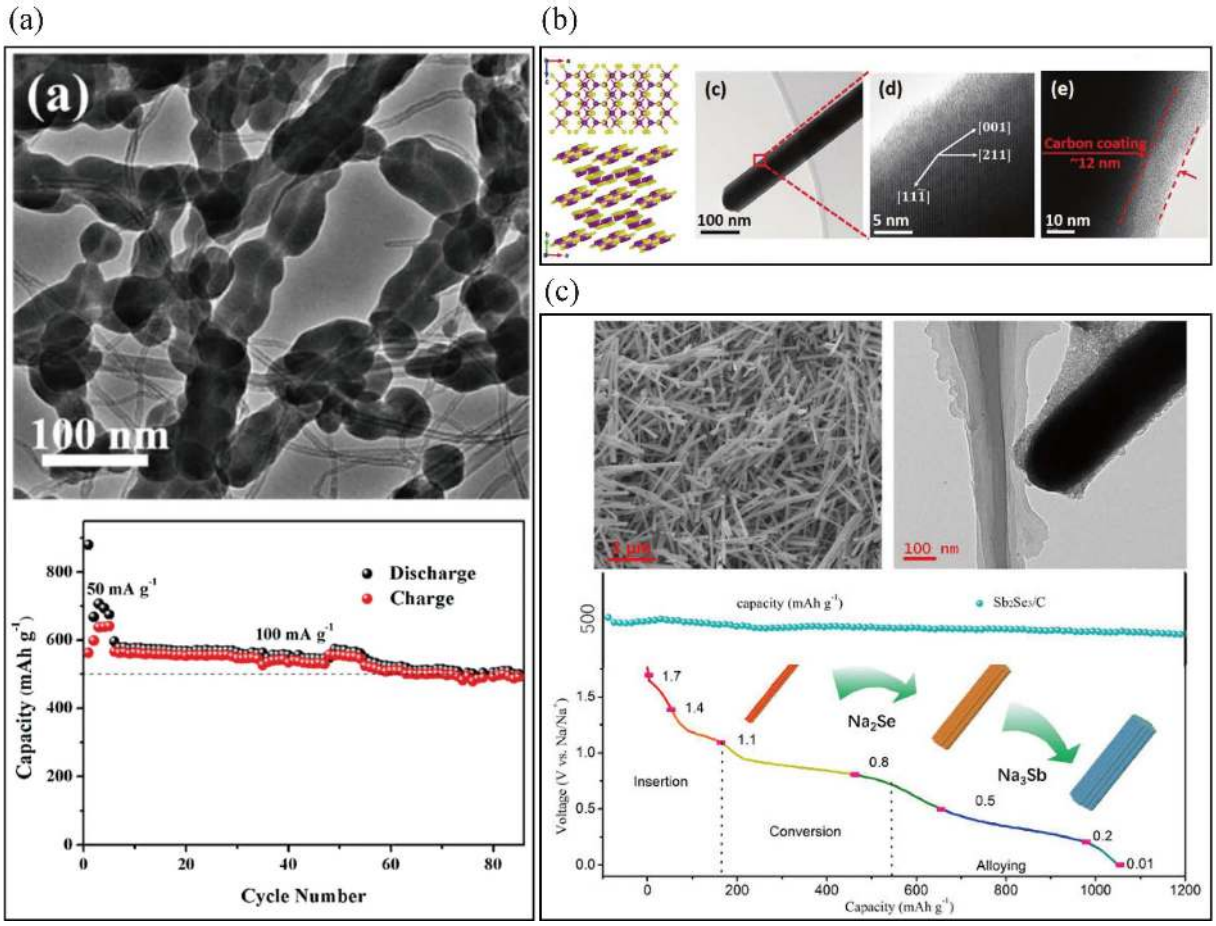

Fig. 6. (a) TEM image and cycle perfroamance of MWCNTs@Sb_2S_3@PPy. Reproduced and modified with permission from ref. 82. Copyright 2016 WILEY-VCH Verlag GmbH & Co. KGaA, Weinheim. (b) Cystalline structure and TEM images of Sb_2S_3 nanorods. Reproduced and modified with permission from ref. 81. Copyright 2016 WILEY-VCH Verlag GmbH & Co. KGaA, Weinheim. (c) Microstructure and reaction mechanism of Sb_2Se_3/C nanocomposite. Reproduced and modified with permission from ref. 87. Copyright 2017 American Chemical Society.

effective diffusion pathways for electrons and Na ions. Kim *et al.* also synthesized cystalline Sb_2S_3 (c-Sb_2S_3) and amorphous Sb_2S_3 (a-Sb_2S_3) nanoparticles via a similar polyol synthetic protocol.[80] The reversible charge capacity of a-Sb_2S_3 was 512 mAh·g^{-1} after 100 cycles with a capacity retention of about 79% (vs the first charge capacity). The c-Sb_2S_3 nanoparticle electrode after 100 cycles exhibited poor electrochemical performance in the cycling and rate tests, although the initial coulombic efficiency of c-Sb_2S_3 was similar to that of a-Sb_2S_3. These were beneficial for reducing the large volume of expansion during sodiation and for enhancing electrical contact. Antimony sulfide (Sb_2S_3) anode materials contained added carbon introduced to provide improved electron paths and stable reaction sites have been reported. These exhibit high reversible specific capacity and stable lifetime characteristics as shown in Fig. 6(a), (b).[82-85]

Since Jiang *et al.* found that Sb_2Se_3@C prepared via high-energy mechanical ball milling of Sb, Se, and carbon black showed a reversible capacity of 650 mAh·g^{-1} at 0.1 A·g^{-1}, antimony selenides and tellurides have become attractive as promising anode materials for NIBs as shown in Fig. 6(c).[86-88,100] One-dimensional Sb_2Se_3/C nanorods grown toward the [001] direction show reversible capacity of 485.2 mAh·g^{-1} after 100 cycles and 311.5 mAh·g^{-1} at a current density of 2.0 A·g^{-1}.[87] Nam *et al.* synthesized the nanostructured Sb_2Te_3-C composites via solid-state reaction and a high-energy ball milling method to investigate the electrochemical properties of the nanocomposites. The Sb_2Te_3-C nanocomposite showed better electrochemical performance with long cycle life, relative to those of the Sb_2Te_3 electrode. The sodiation/de-sodiation mechanisms of the Sb_2Te_3-C nanocomposites, demonstrated using *ex situ* XRD and TEM, confirmed the occurrence of conversion/recombination reactions, whereas Sb_2Te_3 only displayed conversion/non-recombination reactions (no recovery of the original Sb_2Te_3 phase).

3.2.3. The other transition metal chalcogenides

Many other layered transition metal chalcogenides also have been reported for use as anodes for NIBs as shown in Fig. 7.[89-91,94-96] Molybdenum disulfide (MoS_2), a typical layered material, has been intensively investigated as an anode for NIBs. Park *et al.* first studied layered MoS_2 as an intercalation host for room temperature NIBs, although the Na/MoS_2 cell had a discharge capacity of 85 mAh·g^{-1} after 100 cycles, with poor cycle retention. The discharge reaction was interpreted as occurring in two steps: xNa + MoS_2 → Na_xMoS_2. The first step is the intercalation step ($x \leq 0.5$) and next is the conversion step ($0.5 \leq x \leq 1.1$).[101] Layered-structure $MoSe_2$ has a large interlayer distance (~ 0.65 nm), small band gap (~ 1.1 eV), and a theoretical capacity (~ 422 mAh·g^{-1}) that makes $MoSe_2$ promising for use in NIBs. However, there are serious challenges from the low electronic conductivity, large volume change, and high

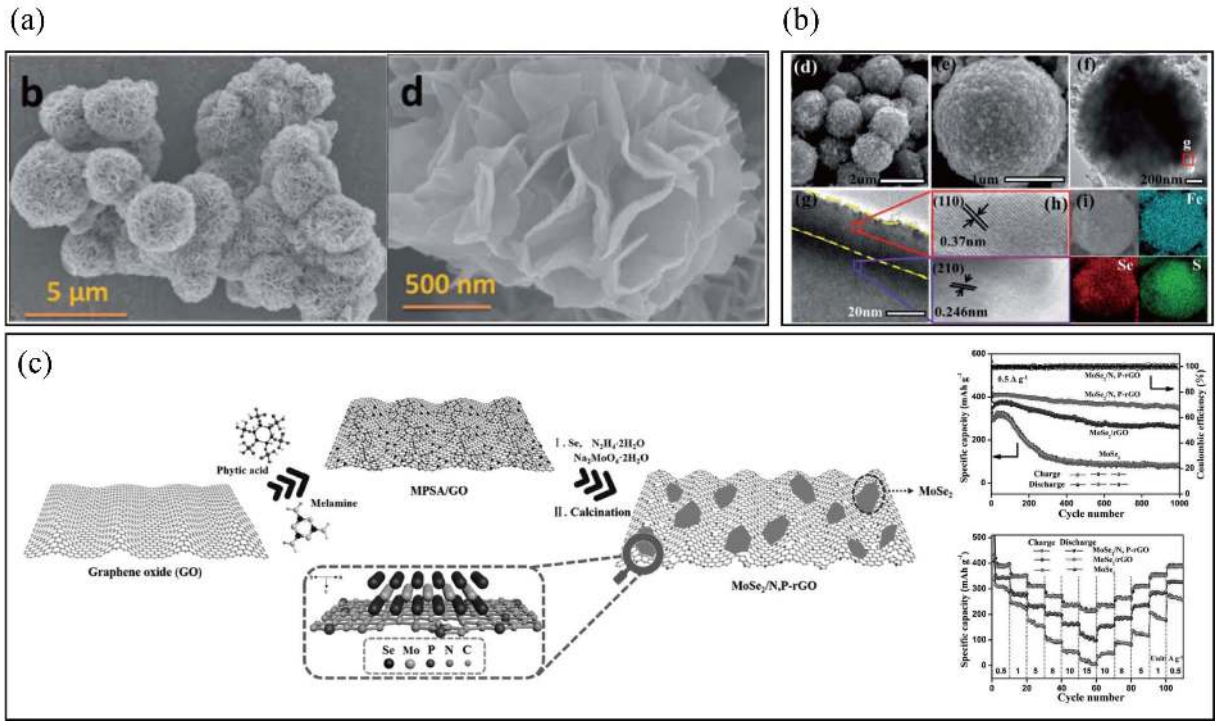

Fig. 7. (a) SEM images of MoS_2 microflowers. Reproduced and modified with permission from ref. 89. Copyright 2015 The Royal Society of Chemistry. (b) Microstructure of FeS_2@FeS_2 microshperes. Reproduced and modified with permission from ref. 93. Copyright 2017 The Royal Society of Chemistry. (c) The preparation process and electrochemical performances of $MoSe_2$/N,P-rGO. Reproduced and modified with permission from ref. 91. Copyright 2017 WILEY-VCH Verlag GmbH & Co. KGaA, Weinheim.

mechanical stress/strain during sodiation/de-sodiation. To solve these problems, $MoSe_2$ homogenously distributed on N,P-doped carbon nanosheets was synthesized using a solvothermal method, followed by high-temperature calcination.[91] This combination presented excellent cycle stability of 378 $mAh{\cdot}g^{-1}$ after 1000 cycles at 0.5 $A{\cdot}g^{-1}$ with 87% cycle retention (vs. the second cycle), and rate capability (the specific capacity at 15 $A{\cdot}g^{-1}$ equals ~ 55% of that of 0.5 $A{\cdot}g^{-1}$). Several non-layered iron sulfides and nickel sulfides for negative electrode materials have been reported, such as FeS_2 and Ni_3S_2.[92,93,102,103] Zhao *et al.* synthesized lychee-like FeS_2@$FeSe_2$ core-shell microspheres, which delivered a reversible discharge capacity of 350 $mAh{\cdot}g^{-1}$ at 1 $A{\cdot}g^{-1}$ after 2700 cycles, and 301.5 $mAh{\cdot}g^{-1}$ at 5 $A{\cdot}g^{-1}$ with a coulombic efficiency of 97%.[93] Such a transition metal chalcogenide electrode had excellent cycle stability and superior rate capability; however, these types of transition metals cannot alloy with sodium, so their reversible capacity is too low to apply for use in high energy-density storage systems.

Recently, germanium (Ge) has become attractive as an anode material for NIBs because of previous reports of its high lithium diffusivity and high lithium storage capacity (until the electrode crystallizes into $Li_{15}Ge_4$) of 1384 $mAh{\cdot}g^{-1}$.[24,104] Chevrier *et al.* calculated the sodiation voltage curves obtained from the DFT total energy for germanium, and got average sodiation voltages of < 0.4 V (vs Na/Na^+). Abel *et al.* synthesized nano columnar germanium thin films by evaporative deposition that had high discharge capacity (403 $mAh{\cdot}g^{-1}$ ≈ that of amorphous $Na_{1.17}Ge$).[105] This exceeded the theoretical value (369 $mAh{\cdot}g^{-1}$) of the fully sodiated NaGe phase). Kim *et al.* first reported germanium disulfide (GeS_2) nanocomposites uniformly distributed on reduced graphene oxide as a promising anode material for NIBs. These were prepared via facile hydrothermal synthesis and a unique carbothermal annealing technique.[96] The GeS_2 hybrid anode yielded a high reversible specific capacity of 805 $mAh{\cdot}g^{-1}$ (> theoretical capacity), an excellent rate capability of 616 $mAh{\cdot}g^{-1}$ at 5 $A{\cdot}g^{-1}$, and a cycle retention of 89.4% after 100 cycles. A combined *ex situ* characterization study revealed that electrochemically driven amorphization plays a key role in achieving efficient sodium storage by accommodating excess sodium ions in the electrode materials. Understanding the sequential conversion-alloying reaction mechanism for GeS_2/rGO hybrid anodes should provide a new approach for developing high-performance energy storage applications.

3.3. Transition metal phosphides

Phosphorus (P) is one of the most promising anode candidates, and studies have demonstrated high theoretical specific capacity of 2596 $mA{\cdot}h^{-1}$ corresponding to final phase Na_3P.[106,107] The operating voltage in NIBs appears to fall in the range 0.0 - 0.5 V, which guarantees high energy density as well as high reversible capacity as shown in Fig. 8a. The platform reaction of phosphorus can be expressed as in reaction (6) and (7) below.

$$\text{Conversion reaction: TM-P}_x + 3x\ Na^+ + 3x\ e^- \leftrightarrow \text{TM} + x\ Na_3P \quad (6)$$

$$\text{Alloying reaction: TM} + y\ Na^+ + y\ e^- \leftrightarrow Na_y\text{-TM alloy} \quad (7)$$

Phosphorus is a Group V non-metallic element in the periodic table and has three allotropes known as white, red, and black phosphorus. White phosphorus begins to ignite in air at 30°C, so it is difficult to use as electrodes and not suitable in terms of safety. To date, red and black P and their composites have been extensively studied as anode materials because of their chemical stability at room temperature and atmospheric pressure. The characteristics of phosphorus anodes for NIBs include 1) high electrochemical performance, 2) cost effectiveness, 3) stability in air (but oxidation in air with a low ignition temperature with white phosphorus, 4) large volume expansion during sodiation, 5) acceptable diffusivity and conductivity of each step (intercalation and alloying), and 6) the need for an *in situ* method to measure the conductivity of intermediate states ($Na_3P \rightarrow Na_2P \rightarrow NaP \rightarrow P$). To solve these problems and allow phosphorus to

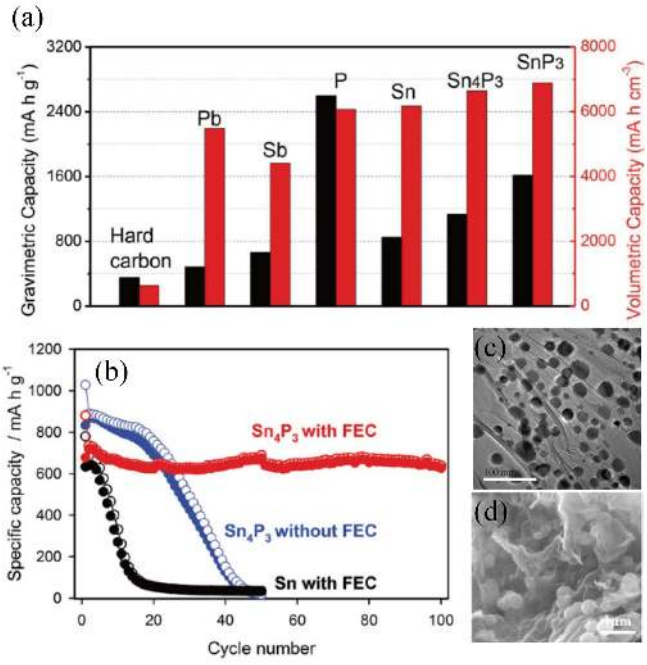

Fig. 8. (a) Theoretical gravimetric and volumetric capacities of various anode mateirals in NIBs. Reproduced and modified with permission from ref. 108. Copyright 2015 WILEY-VCH Verlag GmbH & Co. KGaA, Weinheim. (b) Cycle performance of Sn_4P_3 and Sn electrodes with or without an FEC additive. Reproduced and modified with permission from ref. 109. Copyright 2014 WILEY-VCH Verlag GmbH & Co. KGaA, Weinheim. (c) TEM images of Ni_2P/GNS nanocomposite. Reproduced and modified with permission from ref. 110. Copyright 2016 WILEY-VCH Verlag GmbH & Co. KGaA, Weinheim. (d) SEM images of the H-FeP@C@GR nanocomposite. Reproduced and modified with permission from ref. 111. Copyright 2017 The American Chemical Society.

Table 3. Summary of Transition Metal Phosphide Anodes for Sodium-Ion Batteries

TM-P	Initial charge capacity [mAh·g^{-1}]	Current density [mA·g^{-1}]	Cycle number	Capacity retention [%]	Carbon/GO Content in the anode [%]	Reference
Sn_4P_3	718	100	100	90	0	ref. 109
Sn_4P_3/C	~ 800	100	120	~ 87	24	ref. 112
Sn_4P_3/C	> 750	100	50	~ 700	Unmentioned	ref. 113
$Sn_{4+x}P_3$/Graphene	775	100	100	84	10.4	ref. 114
$Sn_{4+x}P_3$/Sn-P	502	100	100	92.6	0	ref. 115
SnP_3/C	805	150	150	~ 100	~ 20	ref. 108
MoP	> 300	100	800	> 100	23.5	ref. 116
CNT/FeP/C	~ 430	100	100	> 95	~ 50	ref. 117
FeP_4	1145	89.45	30	~ 92	0	ref. 118
FeP/C/Graphene	656	100	250	~ 61	32.4	ref. 111
rGO/CoP/FeP	551.4	100	200	83	Unmentioned	ref. 119
CoP/CNS	598	100	200	83.3	42	ref. 111
CoP/C/Graphene-Ni foam	1163.5	100	100	40.6	> 30	ref. 120
Ni_2P/Graphene	678	200	100	75	21	ref. 121
Cu_3P	~ 200	1000	260	70	0	ref. 122
CuP_2/C	~ 450	200	100	95	20	ref. 123
Se_4P_4	1048	50	60	76.7	0	ref. 124

be utilized as anode material for NIBs, red phosphorus-CNT hybrid nanocomposites were synthesized by simple mixing.[125] These materials provided a reversible capacity of 1675 mAh·g^{-1} with capacity retention of 76.7% over 10 cycles. This suggest that simple synthesis has the potential to allow utilization of red P-CNTs as a promising anode candidate for NIBs with high reversible capacity and low cost. Li *et al.* synthesized red P@CMK-3 hybrid material by melting-diffusion.[126] To avoid the ignition of commercial phosphorus, all synthesis processes were performed in inert gas. Subsequent treatment was heating at 450°C in a sealed vessel for 3 h, after which it was cooled to 260°C for 24 h to convert white P to red P. For the phosphorus-carbon matrix composite, this accommodate large volume change (~ 3 times) of the phosphorus during sodiation/de-sodiation and offered high electron conductivity. However, the reversible capacity based on the mass of red P was only 1020 mAh·g^{-1} after 210 cycles at 5 C-rate (If calculated based on the mass of red P-carbon composite, the reversible capacity was only 370 mAh·g^{-1}; P = 31.54 wt%).

Kim *et al.* first reported ball milling of tin phosphide (Sn_4P_3) for use as a NIB anode. Sn_4P_3 demonstrated excellent electrochemical performance including a reversible capacity of 718 mAh·g^{-1} and stable cycling with negligible capacity fading over 100 cycles as shown in Fig. 8(b).[127] Inspired by this report, many tin-based phosphide nanocomposites have been extensively studied for use in NIBs.[108,112-114,128,129] Huang *et al.* prepared molybdenum phosphide (MoP) nanorods wrapped with a thin carbon layer and disclosed an electrochemical reaction mechanism utilizing *in situ* X-ray diffraction. The nanocomposites exhibited a remarkable rate capability (104.5 mAh·g^{-1} at 1600 mA·g^{-1} even after 10,000 cycles), but the reversible discharge capacity was only 398.4 mAh·g^{-1} at 100 mA·g^{-1} after 800 cycles. Wu *et al.* have developed an assembly and self-tem-plate strategy for the fabrication of Ni_2P@GN hybrids with 3D yolk–shell-like architecture as shown in Fig. 8(c), delivering a high charge capacity of 511 mA h·g^{-1} after 250 cycles with a capacity retention of 93%.[110] CoP nanoparticles uniformly impregnated in N-doped carbon nanosheets were synthesized using a facile calcination method and delivered a reversible capacity of 598 mAh·g^{-1} at 100 mA·g^{-1}.[120] Amorphous Se_4P_4 is promising as anode material, and was synthesized by a mechanical milling technique. It exhibited a high reversible capacity of 1048 mAh·g^{-1}, corresponding to 86% of the theoretical capacity (1217 mAh·g^{-1}) at 50 mA·g^{-1}.[124] The full cell battery (Se_4P_4 anode and $Na_3(VO_{0.5})_2(PO_4)_2F_2$/C cathode) delivered a reversible discharge capacity of 985 mAh·g^{-1} based on the mass of Se_4P_4 with an average output voltage of ~ 2.5 V for the first two cycles. Many other transition metal phosphides such as Cu_3P, CuP_2, CoP, FeP, and Ni_2P have also been revisited because of their potential for utilization in anodes for NIBs.[110,111,117-123] The transition metal phosphide as an promising anode for sodium-ion batteries are reported as shown in Table 3.

4. Summary and Outlook

The qualities that must be provided in battery materials for future energy markets is low-cost, environmental compatibility, safety, and high performance for energy storage.

Due to the increase in the amounts of time that small electronic devices are used and to the development of electric vehicles and large-scale energy storage systems, sodium ion batteries with high energy density are essential. The development of anode materials for sodium ion batteries to overcome the limitations of conventional lithium ion batteries can be expected to provide significant applications for renewable energy devices. The creation of nano-structured electrodes and carbon composites via various synthesis methods has been reported as a strategy to overcome the obstacles affecting safety, high cost, and ease of manufacturing large batteries, which is a vulnerable point of NIB anode materials. Through in-depth understanding of the electrochemical properties of high-performance electrodes and the *in situ* and *ex situ* analysis after charge/discharge processes, it is expected that the sodium secondary battery will not only play a pivotal role in energy related fields, but also will have a large effect on the high value-added technology of the future.

Acknowledgments

This work was supported by a National Research Foundation of Korea (NRF) grant funded by the Korea government (MSIT) (No. 2017R1A2B2010148). It was also supported by the Climate Change Research Hub of KAIST (Grant No. N11180108).

REFERENCES

1. B. Dunn, H. Kamath, and J. M. Tarascon, "Electrical Energy Storage for the Grid: a Battery of Choices," *Science*, **334** [6058] 928-35 (2011).
2. M. Armand and J. M. Tarascon, "Building Better Batteries," *Nature*, **451** [7179] 652-57 (2008).
3. G. E. Blomgren, "The Development and Future of Lithium Ion Batteries," *J. Electrochem. Soc.*, **164** [1] A5019-25 (2017).
4. M. Lazzari and B. Scrosati, "Cyclable Lithium Organic Electrolyte Cell Based on 2 Intercalation Electrodes," *J. Electrochem. Soc.*, **127** [3] 773-74 (1980).
5. D. Larcher and J. M. Tarascon, "Towards Greener and More Sustainable Batteries for Electrical Energy Storage," *Nat. Chem.*, **7** [1] 19-29 (2015).
6. B. Swain, "Cost Effective Recovery of Lithium from Lithium Ion Battery by Reverse Osmosis and Precipitation: a Perspective," *J. Chem. Technol. Biotechnol.*, **93** [2] 311-19 (2018).
7. S. W. Kim, D. H. Seo, X. H. Ma, G. Ceder, and K. Kang, "Electrode Materials for Rechargeable Sodium-Ion Batteries: Potential Alternatives to Current Lithium-Ion Batteries," *Adv. Energy Mater.*, **2** [7] 710-21 (2012).
8. N. Yabuuchi, K. Kubota, M. Dahbi, and S. Komaba, "Research Development on Sodium-Ion Batteries," *Chem. Rev.*, **114** [23] 11636-82 (2014).
9. V. Palomares, P. Serras, I. Villaluenga, K. B. Hueso, J. Carretero-Gonzalez, and T. Rojo, "Na-Ion Batteries, Recent Advances and Present Challenges to Become Low Cost Energy Storage Systems," *Energy Environ. Sci.*, **5** [3] 5884-901 (2012).
10. P. R. Kumar, Y. H. Jung, S. A. Ahad, and D. K. Kim, "A High Rate and Stable Electrode Consisting of a $Na_3V_2O_{2X}(PO_4)_2F_{3-2X}$-rGO Composite with a Cellulose Binder for Sodium-Ion Batteries," *RSC Adv.*, **7** [35] 21820-26 (2017).
11. P. R. Kumar, Y. H. Jung, and D. K. Kim, "Influence of Carbon Polymorphism towards Improved Sodium Storage Properties of $Na_3V_2O_{2x}(PO_4)_2F_{3-2x}$," *J. Solid State Electrochem.*, **21** [1] 223-32 (2017).
12. Y. H. Jung, A. S. Christiansen, R. E. Johnsen, P. Norby, and D. K. Kim, "In Situ X-Ray Diffraction Studies on Structural Changes of a P2 Layered Material during Electrochemical Desodiation/Sodiation," *Adv. Funct. Mater.*, **25** [21] 3227-37 (2015).
13. J. Song, J. Yang, M. H. Alfaruqi, W. Park, S. Park, S. Kim, J. Jo, and J. Kim, "Pyro-Synthesis of $Na_2FeP_2O_7$ Nano-plates as Cathode for Sodium-ion Batteries with Long Cycle Stability," *J. Korean Ceram. Soc.*, **53** [4] 406-10 (2016).
14. J. Y. Hwang, S. T. Myung, and Y. K. Sun, "Sodium-Ion Batteries: Present and Future," *Chem. Soc. Rev.*, **46** [12] 3529-614 (2017).
15. Y. Guo, Y. Wei, H. Li, and T. Zhai, "Layer Structured Materials for Advanced Energy Storage and Conversion," *Small*, **13** [45] 1701649 (2017).
16. H. Y. Kang, Y. C. Liu, K. Z. Cao, Y. Zhao, L. F. Jiao, Y. J. Wang, and H. T. Yuan, "Update on Anode Materials for Na-Ion Batteries," *J. Mater. Chem. A*, **3** [35] 17899-913 (2015).
17. Y. Wen, K. He, Y. J. Zhu, F. D. Han, Y. H. Xu, I. Matsuda, Y. Ishii, J. Cumings, and C. S. Wang, "Expanded Graphite as Superior Anode for Sodium-Ion Batteries," *Nat. Commun.*, **5** 5033 (2014).
18. E. Buiel, and J. R. Dahn, "Li-Insertion in Hard Carbon Anode Materials for Li-Ion Batteries," *Electrochim. Acta*, **45** [1-2] 121-30 (1999).
19. V. L. Chevrier and G. Ceder, "Challenges for Na-Ion Negative Electrodes," *J. Electrochem. Soc.*, **158** [9] A1011-14 (2011).
20. W. Luo, F. Shen, C. Bommier, H. Zhu, X. Ji, and L. Hu, "Na-Ion Battery Anodes: Materials and Electrochemistry," *Acc. Chem. Res.*, **49** [2] 231-40 (2016).
21. Y. Kim, K. H. Ha, S. M. Oh, and K. T. Lee, "High-Capacity Anode Materials for Sodium-Ion Batteries," *Chem. - Eur. J.*, **20** [38] 11980-92 (2014).
22. S. Komaba, Y. Matsuura, T. Ishikawa, N. Yabuuchi, W. Murata, and S. Kuze, "Redox Reaction of Sn-Polyacrylate Electrodes in Aprotic Na Cell," *Electrochem. Commun.*, **21** 65-8 (2012).
23. J. W. Wang, X. H. Liu, S. X. Mao, and J. Y. Huang, "Microstructural Evolution of Tin Nanoparticles during In Situ Sodium Insertion and Extraction," *Nano Lett.*, **12** [11] 5897-902 (2012).
24. S. A. Liu, J. K. Feng, X. F. Bian, Y. T. Qian, J. Liu, and H. Xu, "Nanoporous Germanium as High-Capacity Lithium-Ion Battery Anode," *Nano Energy*, **13** 651-57 (2015).

25. X. W. Li, Z. B. Yang, Y. J. Fu, L. Qiao, D. Li, H. W. Yue, and D. Y. He, "Germanium Anode with Excellent Lithium Storage Performance in a Germanium/Lithium-Cobalt Oxide Lithium-Ion Battery," *ACS Nano*, **9** [2] 1858-67 (2015).
26. L. Baggetto, E. J. M. Hensen, and P. H. L. Notten, "In situ X-ray Absorption Spectroscopy of Germanium Evaporated Thin Film Electrodes," *Electrochim. Acta*, **55** [23] 7074-79 (2010).
27. L. Baggetto and P. H. L. Notten, "Lithium-Ion (De)Insertion Reaction of Germanium Thin-Film Electrodes: An Electrochemical and In Situ XRD Study," *J. Electrochem. Soc.*, **156** [3] A169-A75 (2009).
28. X. T. Lu, E. R. Adkins, Y. He, L. Zhong, L. L. Luo, S. X. Mao, C. M. Wang, and B. A. Korgel, "Germanium as a Sodium Ion Battery Material: In Situ TEM Reveals Fast Sodiation Kinetics with High Capacity," *Chem. Mater.*, **28** [4] 1236-42 (2016).
29. J. W. Wang, X. H. Liu, S. X. Mao, and J. Y. Huang, "Microstructural Evolution of Tin Nanoparticles during in situ Sodium Insertion and Extraction," *Nano Lett.*, **12** [11] 5897-902 (2012).
30. F. Wan, J. Z. Guo, X. H. Zhang, J. P. Zhang, H. Z. Sun, Q. Y. Yan, D. X. Han, L. Niu, and X. L. Wu, "In Situ Binding Sb Nanospheres on Graphene via Oxygen Bonds as Superior Anode for Ultrafast Sodium-Ion Batteries," *ACS Appl. Mater. Interfaces*, **8** [12] 7790-99 (2016).
31. X. L. Zhou, Y. R. Zhong, M. Yang, M. Hu, J. P. Wei, and Z. Zhou, "Sb Nanoparticles Decorated N-rich Carbon Nanosheets as Anode Materials for Sodium Ion Batteries with Superior Rate Capability and Long Cycling Stability," *Chem. Commun.*, **50** [85] 12888-91 (2014).
32. L. Luo, H. Qiao, W. Z. Xu, D. W. Li, J. D. Zhu, C. Chen, Y. Lu, P. Zhu, X. W. Zhang, and Q. F. Wei, "Tin Nanoparticles Embedded in Ordered Mesoporous Carbon as High-Performance Anode for Sodium-Ion Batteries," *J. Solid State Electrochem.*, **21** [5] 1385-95 (2017).
33. Q. Q. Yang, J. Zhou, G. Q. Zhang, C. Guo, M. Li, Y. C. Zhu, and Y. T. Qian, "Sb Nanoparticles Uniformly Dispersed in 1-D N-doped Porous Carbon as Anodes for Li-Ion and Na-Ion Batteries," *J. Mater. Chem. A*, **5** [24] 12144-48 (2017).
34. Y. X. Wang, Y. G. Lim, M. S. Park, S. L. Chou, J. H. Kim, H. K. Liu, S. X. Dou, and Y. J. Kim, "Ultrafine SnO_2 Nanoparticle Loading onto Reduced Graphene Oxide as Anodes for Sodium-Ion Batteries with Superior Rate and Cycling Performances," *J. Mater. Chem. A*, **2** [2] 529-34 (2014).
35. H. W. Song, N. Li, H. Cui, and C. X. Wang, "Enhanced Capability and Cyclability of SnO_2-Graphene Oxide Hybrid Anode by Firmly Anchored SnO_2 Quantum Dots," *J. Mater. Chem. A*, **1** [26] 7558-62 (2013).
36. J. Patra, H. C. Chen, C. H. Yang, C. T. Hsieh, C. Y. Su, and J. K. Chang, "High Dispersion of 1-nm SnO_2 Particles between Graphene Nanosheets Constructed Using Supercritical CO_2 Fluid for Sodium-Ion Battery Anodes," *Nano Energy*, **28** 124-34 (2016).
37. R. S. Kalubarme, J. Y. Lee, and C. J. Park, "Carbon Encapsulated Tin Oxide Nanocomposites: An Efficient Anode for High Performance Sodium-Ion Batteries," *ACS Appl. Mater. Interfaces*, **7** [31] 17226-37 (2015).
38. X. Xie, S. Chen, B. Sun, C. Wang, and G. Wang, "3D Networked Tin Oxide/Graphene Aerogel with a Hierarchically Porous Architecture for High-Rate Performance Sodium-Ion Batteries," *ChemSusChem*, **8** [17] 2948-55 (2015).
39. Z. D. Huang, H. S. Hou, G. Q. Zou, J. Chen, Y. Zhang, H. X. Liao, S. M. Li, and X. B. Ji, "3D Porous Carbon Encapsulated SnO_2 Nanocomposite for Ultrastable Sodium Ion Batteries," *Electrochim. Acta*, **214** 156-64 (2016).
40. G. Z. Wang, J. M. Feng, L. Dong, X. F. Li, and D. J. Li, "SnO_2 Particles Anchored on N-Doped Graphene Surface as Sodium-Ion Battery Anode with Enhanced Electrochemical Capability," *Appl. Surf. Sci.*, **396** 269-77 (2017).
41. H. S. Hou, M. J. Jing, Y. C. Yang, Y. Zhang, W. X. Song, X. M. Yang, J. Chen, Q. Y. Chen, and X. B. Ji, "Antimony Nanoparticles Anchored on Interconnected Carbon Nanofibers Networks as Advanced Anode Material for Sodium-Ion Batteries," *J. Power Sources*, **284** 227-35 (2015).
42. D. H. Nam, K. S. Hong, S. J. Lim, M. J. Kim, and H. S. Kwon, "High-Performance Sb/Sb_2O_3 Anode Materials Using a Polypyrrole Nanowire Network for Na-Ion Batteries," *Small*, **11** [24] 2885-92 (2015).
43. K. S. Hong, D. H. Nam, S. J. Lim, D. Sohn, T. H. Kim, and H. Kwon, "Electrochemically Synthesized Sb/Sb_2O_3 Composites as High-Capacity Anode Materials Utilizing a Reversible Conversion Reaction for Na-Ion Batteries," *ACS Appl. Mater. Interface*, **7** [31] 17264-71 (2015).
44. G. Z. Wang, J. M. Feng, L. Dong, X. F. Li, and D. J. Li, "Antimony (IV) Oxide Nanorods/Reduced Graphene Oxide as the Anode Material of Sodium-ion Batteries with Excellent Electrochemical Performance," *Electrochim. Acta*, **240** 203-14 (2017).
45. J. Fei, Y. L. Cui, J. Y. Li, Z. W. Xu, J. Yang, R. Y. Wang, Y. Y. Cheng, and J. F. Hang, "A Flexible Sb_2O_3/Carbon Cloth Composite as a Free-Standing High Performance Anode for Sodium Ion Batteries," *Chem. Commun.*, **53** [98] 13165-67 (2017).
46. M. J. Hu, Y. Z. Jiang, W. P. Sun, H. T. Wang, C. H. Jin, and M. Yan, "Reversible Conversion-Alloying of Sb_2O_3 as a High-Capacity, High-Rate, and Durable Anode for Sodium Ion Batteries," *ACS Appl. Mater. Interface*, **6** [21] 19449-55 (2014).
47. L. Zhao, H. L. Pan, Y. S. Hu, H. Li, and L. Q. Chen, "Spinel Lithium Titanate ($Li_4Ti_5O_{12}$) as Novel Anode Material for Room-Temperature Sodium-Ion Battery," *Chin. Phys. B*, **21** [2] (2012).
48. Y. Sun, L. Zhao, H. L. Pan, X. Lu, L. Gu, Y. S. Hu, H. Li, M. Armand, Y. Ikuhara, L.Q. Chen, and X. J. Huang, "Direct Atomic-Scale Confirmation of Three-Phase Storage Mechanism in $Li_4Ti_5O_{12}$ Anodes for Room-Temperature Sodium-Ion Batteries," *Nat. Commun.*, **4** 2878 (2013).
49. P. Senguttuvan, G. Rousse, V. Seznec, J. M. Tarascon, and M. R. Palacin, "$Na_2Ti_3O_7$: Lowest Voltage Ever Reported Oxide Insertion Electrode for Sodium Ion Batteries," *Chem. Mater.*, **23** [18] 4109-11 (2011).
50. Y. S. Wang, X. Q. Yu, S. Y. Xu, J. M. Bai, R. J. Xiao, Y. S. Hu, H. Li, X. Q. Yang, L. Q. Chen, and X. J. Huang, "A

Zero-Strain Layered Metal Oxide as the Negative Electrode for Long-Life Sodium-Ion Batteries," *Nat. Commun.*, **4** [2365] 1-8 (2013).
51. D. B. S. H. Kim, C. Kim, and J. G. Lee, "Na-Ion Anode Based on Na(Li,Ti)O_2 System: Effects of Mg Addition," *J. Korean Ceram. Soc.*, **53** [3] 282-87 (2016).
52. A. Rudola, K. Saravanan, S. Devaraj, H. Gong, and P. Balaya, "$Na_2Ti_6O_{13}$: A Potential Anode for Grid-Storage Sodium-Ion Batteries," *Chem. Commun.*, **49** [67] 7451-53 (2013).
53. M. Shirpour, J. Cabana, and M. Doeff, "New Materials Based on a Layered Sodium Titanate for Dual Electrochemical Na and Li Intercalation Systems," *Energy Environ. Sci.*, **6** [8] 2538-47 (2013).
54. R. Alcantara, M. Jaraba, P. Lavela, and J. L. Tirado, "$NiCo_2O_4$ Spinel: First Report on a Transition Metal Oxide for the Negative Electrode of Sodium-Ion Batteries," *Chem. Mater.*, **14** [7] 2847-48 (2002).
55. R. S. Kalubarme, A. I. Inamdar, D. S. Bhange, H. Im, S. W. Gosavi, and C. J. Park, "Nickel-Titanium Oxide as a Novel Anode Material for Rechargeable Sodium-Ion Batteries," *J. Mater. Chem. A*, **4** [44] 17419-30 (2016).
56. S. Komaba, T. Mikumo, N. Yabuuchi, A. Ogata, H. Yoshida, and Y. Yamada, "Electrochemical Insertion of Li and Na Ions into Nanocrystalline Fe_3O_4 and α-Fe_2O_3 for Rechargeable Batteries," *J. Electrochem. Soc.*, **157** [1] A60-5 (2010).
57. P. R. Kumar, Y. H. Jung, K. K. Bharathi, C. H. Lim, and D. K. Kim, "High Capacity and Low Cost Spinel Fe_3O_4 for the Na-Ion Battery Negative Electrode Materials," *Electrochim. Acta*, **146** 503-10 (2014).
58. D. S. Li, D. Yan, X. J. Zhang, J. B. Li, T. Lu, and L. K. Pan, "Porous CuO/Reduced Graphene Oxide Composites Synthesized from Metal-Organic Frameworks as Anodes for High-Performance Sodium-Ion Batteries," *J. Colloid Interface Sci.*, **497** 350-58 (2017).
59. G. Longoni, M. Fiore, J. H. Kim, Y. H. Jung, D. K. Kim, C. M. Mari, and R. Ruffo, "Co_3O_4 Negative Electrode Material for Rechargeable Sodium Ion Batteries: An Investigation of Conversion Reaction Mechanism and Morphology-Performances Correlations," *J. Power Sources*, **332** 42-50 (2016).
60. S. Meng, D.L. Zhao, L. L. Wu, Z. W. Ding, X. W. Cheng, and T. Hu, "Fe_2O_3/Nitrogen-Doped Graphene Nanosheet Nanocomposites as Anode Materials for Sodium-Ion Batteries with Enhanced Electrochemical Performance," *J. Alloys Compd.*, **737** 130-35 (2018).
61. M. M. Rahman, I. Sultana, Z. Q. Chen, M. Srikanth, L. H. Li, X. J. J. Dai, and Y. Chen, "Ex situ Electrochemical Sodiation/Desodiation Observation of Co_3O_4 Anchored Carbon Nanotubes: A High Performance Sodium-Ion Battery Anode Produced by Pulsed Plasma in a Liquid," *Nanoscale*, **7** [30] 13088-95 (2015).
62. X. J. Wang, Y. C. Liu, Y. J. Wang, and L. F. Jiao, "CuO Quantum Dots Embedded in Carbon Nanofibers as Binder-Free Anode for Sodium Ion Batteries with Enhanced Properties," *Small*, **12** [35] 4865-72 (2016).
63. S. M. Oh, S. T. Myung, C. S. Yoon, J. Lu, J. Hassoun, B. Scrosati, K. Amine, and Y. K. Sun, "Advanced Na[$Ni_{0.25}Fe_{0.5}Mn_{0.25}$]$O_2$/C-$Fe_3O_4$ Sodium-Ion Batteries Using EMS Electrolyte for Energy Storage," *Nano Lett.*, **14** [3] 1620-26 (2014).
64. J. Pan, N. N. Wang, Y. L. Zhou, X. F. Yang, W. Y. Zhou, Y. T. Qian, and J. Yang, "Simple Synthesis of a Porous Sb/Sb_2O_3 Nanocomposite for a High-Capacity Anode Material in Na-Ion Batteries," *Nano Res.*, **10** [5] 1794-803 (2017).
65. D. S. Li, D. Yana, J. Q. Ma, W. Qin, X. J. Zhang, T. Lu, and L. K. Pan, "One-Step Microwave-Assisted Synthesis of Sb_2O_3/Reduced Graphene Oxide Composites as Advanced Anode Materials for Sodium-Ion Batteries," *Ceram. Int.*, **42** [14] 15634-42 (2016).
66. Z. N. Guo, F. Sun, and W. X. Yuan, "Chemical Intercalations in Layered Transition Metal Chalcogenides: Syntheses, Structures, and Related Properties," *Cryst. Growth Des.*, **17** [4] 2238-53 (2017).
67. M. Pumera, Z. Sofer, and A. Ambrosi, "Layered Transition Metal Dichalcogenides for Electrochemical Energy Generation and Storage," *J. Mater. Chem. A*, **2** [24] 8981-87 (2014).
68. L. Wu, X. H. Hu, J. F. Qian, F. Pei, F. Y. Wu, R. J. Mao, X. P. Ai, H. X. Yang, and Y. L. Cao, "A Sn-SnS-C Nanocomposite as Anode Host Materials for Na-Ion Batteries," *J. Mater. Chem. A*, **1** [24] 7181-84 (2013).
69. L. Wu, H. Y. Lu, L. F. Xiao, J. F. Qian, X. P. Ai, H. X. Yang, and Y. L. Cao, "A Tin(II) Sulfide-Carbon Anode Material Based on Combined Conversion and Alloying Reactions for Sodium-Ion Batteries," *J. Mater. Chem. A*, **2** [39] 16424-28 (2014).
70. T. Zhou, W. K. Pang, C. Zhang, J. Yang, Z. Chen, H. K. Liu, and Z. Guo, "Enhanced Sodium-Ion Battery Performance by Structural Phase Transition from Two-Dimensional Hexagonal-SnS_2 to Orthorhombic-SnS," *ACS Nano*, **8** [8] 8323-33 (2014).
71. B. Qu, C. Ma, G. Ji, C. Xu, J. Xu, Y. S. Meng, T. Wang, and J. Y. Lee, "Layered SnS_2-Reduced Graphene Oxide Composite - A High-Capacity, High-Rate, and Long-Cycle Life Sodium-Ion Battery Anode Material," *Adv. Mater.*, **26** [23] 3854-59 (2014).
72. Y. D. Zhang, P. Y. Zhu, L. L. Huang, J. Xie, S. C. Zhang, G. S. Cao, and X. B. Zhao, "Few-Layered SnS_2 on Few-Layered Reduced Graphene Oxide as Na-Ion Battery Anode with Ultralong Cycle Life and Superior Rate Capability," *Adv. Funct. Mater.*, **25** [3] 481-89 (2015).
73. F. Z. Tu, X. Xu, P. Z. Wang, L. Si, X. S. Zhou, and J. C. Bao, "A Few-Layer SnS_2/Reduced Graphene Oxide Sandwich Hybrid for Efficient Sodium Storage," *J. Phys. Chem. C*, **121** [6] 3261-69 (2017).
74. J. H. Kim, Y. H. Jung, J. H. Yun, P. Ragupathy, and D. K. Kim, "Enhancing the Sequential Conversion-Alloying Reaction of Mixed Sn-S Hybrid Anode for Efficient Sodium Storage by a Carbon Healed Graphene Oxide," *Small*, **14** [4] 1702605 (2018).
75. Y. Kim, Y. Kim, Y. Park, Y. N. Jo, Y. J. Kim, N. S. Choi, and K. T. Lee, "SnSe Alloy as a Promising Anode Material for Na-Ion Batteries," *Chem. Commun.*, **51** [1] 50-3 (2015).
76. Z. A. Zhang, X. X. Zhao, and J. Li, "SnSe/Carbon Nanocomposite Synthesized by High Energy Ball Milling as an

Anode Material for Sodium-Ion and Lithium-Ion Batteries," *Electrochim. Acta*, **176** 1296-301 (2015).
77. F. Zhang, C. Xia, J. J. Zhu, B. Ahmed, H. F. Liang, D. B. Velusamy, U. Schwingenschlogl, and H. N. Alshareef, "$SnSe_2$ 2D Anodes for Advanced Sodium Ion Batteries," *Adv. Energy Mater.*, **6** [22] 1601188 (2016).
78. A. R. Park and C. M. Park, "Cubic Crystal-Structured SnTe for Superior Li- and Na-Ion Battery Anodes," *ACS Nano*, **11** [6] 6074-84 (2017).
79. Y. Zhu, P. Nie, L. Shen, S. Dong, Q. Sheng, H. Li, H. Luo, and X. Zhang, "High Rate Capability and Superior Cycle Stability of a Flower-like Sb_2S_3 Anode for High-Capacity Sodium Ion Batteries," *Nanoscale*, **7** [7] 3309-15 (2015).
80. S. M. Hwang, J. Kim, Y. Kim, and Y. Kim, "Na-Ion Storage Performance of Amorphous Sb_2S_3 Nanoparticles: Anode for Na-Ion Batteries and Seawater Flow Batteries," *J. Mater. Chem. A*, **4** [46] 17946-51 (2016).
81. S. S. Yao, J. Cui, Z. H. Lu, Z .L. Xu, L. Qin, J. Q. Huang, Z. Sadighi, F. Ciucci, and J. K. Kim, "Unveiling the Unique Phase Transformation Behavior and Sodiation Kinetics of 1D van der Waals Sb_2S_3 Anodes for Sodium Ion Batteries," *Adv. Energy Mater.*, **7** [8] 1602149 (2017).
82. S. Wang, S. Yuan, Y. B. Yin, Y. H. Zhu, X. B. Zhang, and J. M. Yan, "Green and Facile Fabrication of MWNTs@Sb_2S_3@PPy Coaxial Nanocables for High-Performance Na-Ion Batteries," *Part. Part. Syst. Charact.*, **33** [8] 493-99 (2016).
83. Y. Zhao and A. Manthiram, "Amorphous Sb_2S_3 Embedded in Graphite: A High-Rate, Long-Life Anode Material for Sodium-Ion Batteries," *Chem. Commun.,* **51** [67] 13205-8 (2015).
84. D. Y. W. Yu, P. V. Prikhodchenko, C. W. Mason, S. K. Batabyal, J. Gun, S. Sladkevich, A. G. Medvedev, and O. Lev, "High-Capacity Antimony Sulphide Nanoparticle-Decorated Graphene Composite as Anode for Sodium-Ion Batteries," *Nat. Commun.*, **4** 2922 (2013).
85. X. Xiong, G. Wang, Y. Lin, Y. Wang, X. Ou, F. Zheng, C. Yang, J. H. Wang, and M. Liu, "Enhancing Sodium Ion Battery Performance by Strongly Binding Nanostructured Sb_2S_3 on Sulfur-Doped Graphene Sheets," *ACS Nano*, **10** [12] 10953-59 (2016).
86. W. Luo, A. Calas, C. Tang, F. Li, L. Zhou, and L. Mai, "Ultralong Sb_2Se_3 Nanowire-Based Free-Standing Membrane Anode for Lithium/Sodium Ion Batteries," *ACS Appl. Mater. Interfaces*, **8** [51] 35219-26 (2016).
87. P. Ge, X. Cao, H. Hou, S. Li, and X. Ji, "Rodlike Sb_2Se_3 Wrapped with Carbon: The Exploring of Electrochemical Properties in Sodium-Ion Batteries," *ACS Appl. Mater. Interfaces*, **9** [40] 34979-89 (2017).
88. K. H. Nam, J. H. Choi, and C. M. Park, "Highly Reversible Na-Ion Reaction in Nanostructured Sb_2Te_3-C Composites as Na-Ion Battery Anodes," *J. Electrochem. Soc.*, **164** [9] A2056-64 (2017).
89. P. R. Kumar, Y. H. Jung, and D. K. Kim, "High Performance of MoS_2 Microflowers with a Water-Based Binder as an Anode for Na-Ion Batteries," *RSC Adv.*, **5** [97] 79845-51 (2015).
90. C. B. Zhu, X. K. Mu, P. A. van Aken, Y. Yu, and J. Maier, "Single-Layered Ultrasmall Nanoplates of MoS_2 Embedded in Carbon Nanofibers with Excellent Electrochemical Performance for Lithium and Sodium Storage," *Angew. Chem., Int. Ed.*, **53** [8] 2152-56 (2014).
91. F. E. Niu, J. Yang, N. N. Wang, D. P. Zhang, W. L. Fan, J. Yang, and Y. T. Qian, "$MoSe_2$-Covered N,P-Doped Carbon Nanosheets as a Long-Life and High-Rate Anode Material for Sodium-Ion Batteries," *Adv. Funct. Mater.*, **27** [23] 1700522 (2017).
92. K. Zhang, M. Park, L. M. Zhou, G. H. Lee, J. Shin, Z. Hu, S. L. Chou, J. Chen, and Y. M. Kang, "Cobalt-Doped FeS_2 Nanospheres with Complete Solid Solubility as a High-Performance Anode Material for Sodium-Ion Batteries," *Angew. Chem., Int. Ed.*, **55** [41] 12822-26 (2016).
93. W. X. Zhao, C. X. Guo, and C. M. Li, "Lychee-like FeS_2@$FeSe_2$ Core-Shell Microspheres Anode in Sodium Ion Batteries for Large Capacity and Ultralong Cycle Life," *J. Mater. Chem. A*, **5** [36] 19195-202 (2017).
94. Q. Guo, Y. Ma, T. Chen, Q. Xia, M. Yang, H. Xia, and Y. Yu, "Cobalt Sulfide Quantum Dot Embedded N/S-Doped Carbon Nanosheets with Superior Reversibility and Rate Capability for Sodium-Ion Batteries," *ACS Nano*, **11** [12] 12658-67 (2017).
95. Y. N. Ko, S. H. Choi, and Y. C. Kang, "Hollow Cobalt Selenide Microspheres: Synthesis and Application as Anode Materials for Na-Ion Batteries," *ACS Appl. Mater. Interface*, **8** [10] 6449-56 (2016).
96. J. H. Kim, J. H. Yun, and D. K. Kim, "A Robust Approach for Efficient Sodium Storage of GeS_2 Hybrid Anode by Electrochemically Driven Amorphization," *Adv. Energy Mater.*, 1703499 (2018).
97. X. Y. Yu, L. Yu, and X. W. Lou, "Metal Sulfide Hollow Nanostructures for Electrochemical Energy Storage," *Adv. Energy Mater.*, **6** [3] 1501333 (2016).
98. X. Huang, Z. Zeng, and H. Zhang, "Metal Dichalcogenide Nanosheets: Preparation, Properties and Applications," *Chem. Soc. Rev.*, **42** [5] 1934-46 (2013).
99. X. Rui, H. Tan, and Q. Yan, "Nanostructured Metal Sulfides for Energy Storage," *Nanoscale*, **6** [17] 9889-924 (2014).
100. W. Li, M. Zhou, H. M. Li, K. L. Wang, S. J. Cheng, and K. Jiang, "Carbon-Coated Sb_2Se_3 Composite as Anode Material for Sodium Ion Batteries," *Electrochem. Commun.*, **60** 74-7 (2015).
101. J. Park, J. S. Kim, J. W. Park, T. H. Nam, K. W. Kim, J. H. Ahn, G. Wang, and H. J. Ahn, "Discharge Mechanism of MoS_2 for Sodium Ion Battery: Electrochemical Measurements and Characterization," *Electrochim. Acta*, **92** 427-32 (2013).
102. X. S. Song, X. F. Li, Z. M. Bai, B. Yan, D. J. Li, and X. L. Sun, "Morphology-Dependent Performance of Nanostructured Ni_3S_2/Ni Anode Electrodes for High Performance Sodium Ion Batteries," *Nano Energy*, **26** 533-40 (2016).
103. Y. Han, S. Y. Liu, L. Cui, L. Xu, J. Xie, X. K. Xia, W. K. Hao, B. Wang, H. Li, and J. Gao, "Graphene-Immobilized Flower-like Ni_3S_2 Nanoflakes as a Stable Binder-Free Anode Material for Sodium-Ion Batteries," *Int. J. Miner., Metall. Mater.*, **25** [1] 88-93 (2018).
104. S. Choi, Y. G. Cho, J. Kim, N. S. Choi, H. K. Song, G. Wang, and S. Park, "Mesoporous Germanium Anode Mate-

rials for Lithium-Ion Battery with Exceptional Cycling Stability in Wide Temperature Range," *Small*, **13** [13] 1603045 (2017).
105. P. R. Abel, Y. M. Lin, T. de Souza, C. Y. Chou, A. Gupta, J. B. Goodenough, G. S. Hwang, A. Heller, and C. B. Mullins, "Nanocolumnar Germanium Thin Films as a High-Rate Sodium-Ion Battery Anode Material," *J. Phys. Chem. C*, **117** [37] 18885-90 (2013).
106. M. Mayo, K. J. Griffith, C. J. Pickard, and A. J. Morris, "Ab Initio Study of Phosphorus Anodes for Lithium- and Sodium-Ion Batteries," *Chem. Mater.*, **28** [7] 2011-21 (2016).
107. M. Dahbi, N. Yabuuchi, M. Fukunishi, K. Kubota, K. Chihara, K. Tokiwa, X. F. Yu, H. Ushiyama, K. Yamashita, J. Y. Son, Y. T. Cui, H. Oji, and S. Komaba, "Black Phosphorus as a High-Capacity, High-Capability Negative Electrode for Sodium-Ion Batteries: Investigation of the Electrode/Interface," *Chem. Mater.*, **28** [6] 1625-35 (2016).
108. X. L. Fan, J. F. Mao, Y. J. Zhu, C. Luo, L. M. Suo, T. Gao, F. D. Han, S. C. Liou, and C. S. Wang, "Superior Stable Self-Healing SnP_3 Anode for Sodium-Ion Batteries," *Adv. Energy Mater.*, **5** [18] 1500174 (2015).
109. Y. Kim, Y. Kim, A. Choi, S. Woo, D. Mok, N. S. Choi, Y. S. Jung, J. H. Ryu, S. M. Oh, and K. T. Lee, "Tin Phosphide as a Promising Anode Material for Na-Ion Batteries," *Adv. Mater.*, **26** [24] 4139-44 (2014).
110. C. Wu, P. Kopold, P. A. van Aken, J. Maier, and Y. Yu, "High Performance Graphene/Ni_2P Hybrid Anodes for Lithium and Sodium Storage through 3D Yolk-Shell-Like Nanostructural Design," *Adv. Mater.*, **29** [3] 1604015 (2017).
111. X. J. Wang, K. Chen, G. Wang, X. J. Liu, and H. Wang, "Rational Design of Three-Dimensional Graphene Encapsulated with Hollow FeP@Carbon Nanocomposite as Outstanding Anode Material for Lithium Ion and Sodium Ion Batteries," *ACS Nano*, **11** [11] 11602-16 (2017).
112. X. L. Fan, T. Gao, C. Luo, F. Wang, J. K. Hu, and C. S. Wang, "Superior Reversible Tin Phosphide-Carbon Spheres for Sodium Ion Battery Anode," *Nano Energy*, **38** 350-57 (2017).
113. L. B. Ma, P. J. Yan, S. K. Wu, G. Y. Zhu, and Y. L. Shen, "Engineering Tin Phosphides@Carbon Yolk-Shell Nanocube Structures as a Highly Stable Anode Material for Sodium-Ion Batteries," *J. Mater. Chem. A*, **5** [32] 16994-7000 (2017).
114. Q. Li, Z. Q. Li, Z. W. Zhang, C. X. Li, J. Y. Ma, C. X. Wang, X. L. Ge, S. H. Dong, and L. W. Yin, "Low-Temperature Solution-Based Phosphorization Reaction Route to Sn_4P_3/Reduced Graphene Oxide Nanohybrids as Anodes for Sodium Ion Batteries," *Adv. Energy Mater.*, **6** [15] 1600376 (2016).
115. W. J. Li, S. L. Chou, J. Z. Wang, J. H. Kim, H. K. Liu, and S. X. Dou, "$Sn_{4+x}P_3$ @ Amorphous Sn-P Composites as Anodes for Sodium-Ion Batteries with Low Cost, High Capacity, Long Life, and Superior Rate Capability," *Adv. Mater.*, **26** [24] 4037-42 (2014).
116. Z. D. Huang, H. S. Hou, C. Wang, S. M. Li, Y. Zhang, and X. B. Ji, "Molybdenum Phosphide: A Conversion-type Anode for Ultralong-Life Sodium-Ion Batteries," *Chem. Mater.*, **29** [17] 7313-22 (2017).
117. F. Han, C. Y. J. Tan, and Z. Q. Gao, "Improving the Specific Capacity and Cyclability of Sodium-Ion Batteries by Engineering a Dual-Carbon Phase-Modified Amorphous and Mesoporous Iron Phosphide," *ChemElectroChem*, **3** [7] 1054-62 (2016).
118. W. J. Zhang, M. Dahbi, S. Amagasa, Y. Yamada, and S. Komaba, "Iron Phosphide as Negative Electrode Material for Na-Ion Batteries," *Electrochem. Commun.*, **69** 11-4 (2016).
119. Z. Q. Li, L. Y. Zhang, X. L. Ge, C. X. Li, S. H. Dong, C. X. Wang, and L. W. Yin, "Core-Shell Structured CoP/FeP Porous Microcubes Interconnected by Reduced Graphene Oxide as High Performance Anodes for Sodium Ion Batteries," *Nano Energy*, **32** 494-502 (2017).
120. K. Zhang, M. Park, J. Zhang, G. H. Lee, J. Shin, and Y. M. Kang, "Cobalt Phosphide Nanoparticles Embedded in Nitrogen-Doped Carbon Nanosheets: Promising Anode Material with High Rate Capability and Long Cycle Life for Sodium-Ion Batteries," *Nano Res.*, **10** [12] 4337-50 (2017).
121. X. L. Ge, Z. Q. Li, and L. W. Yin, "Metal-Organic Frameworks Derived Porous Core/ShellCoP@C Polyhedrons Anchored on 3D Reduced Graphene Oxide Networks as Anode for Sodium- Ion Battery," *Nano Energy*, **32** 117-24 (2017).
122. M. P. Fan, Y. Chen, Y. H. Xie, T. Z. Yang, X. W. Shen, N. Xu, H. Y. Yu, and C. L. Yan, "Half-Cell and Full-Cell Applications of Highly Stable and Binder-Free Sodium Ion Batteries Based on Cu_3P Nanowire Anodes," *Adv. Funct. Mater.*, **26** [28] 5019-27 (2016).
123. S. O. Kim and A. Manthiram, "The Facile Synthesis and Enhanced Sodium-Storage Performance of a Chemically Bonded CuP_2/C Hybrid Anode," *Chem. Commun.,* **52** [23] 4337-40 (2016).
124. Y. Y. Lu, P. F. Zhou, K. X. Lei, Q. Zhao, Z. L. Tao, and J. Chen, "Selenium Phosphide (Se_4P_4) as a New and Promising Anode Material for Sodium-Ion Batteries," *Adv. Energy Mater.*, **7** [7] 1601973 (2017).
125. W. J. Li, S. L. Chou, J. Z. Wang, H. K. Liu, and S. X. Dou, "Simply Mixed Commercial Red Phosphorus and Carbon Nanotube Composite with Exceptionally Reversible Sodium-Ion Storage," *Nano Lett.*, **13** [11] 5480-84 (2013).
126. W. Li, Z. Yang, M. Li, Y. Jiang, X. Wei, X. Zhong, L. Gu, and Y. Yu, "Amorphous Red Phosphorus Embedded in Highly Ordered Mesoporous Carbon with Superior Lithium and Sodium Storage Capacity," *Nano Lett.*, **16** [3] 1546-53 (2016).
127. Y. Kim, Y. Kim, A. Choi, S. Woo, D. Mok, N. S. Choi, Y. S. Jung, J. H. Ryu, S. M. Oh, and K. T. Lee, "Tin Phosphide as a Promising Anode Material for Na-Ion Batteries," *Adv. Mater.*, **26** [24] 4139-44 (2014).
128. J. Liu, P. Kopold, C. Wu, P. A. van Aken, J. Maier, and Y. Yu, "Uniform Yolk-Shell Sn_4P_3@C Nanospheres as High-Capacity and Cycle-Stable Anode Materials for Sodium-Ion Batteries," *Energy Environ. Sci.*, **8** [12] 3531-38 (2015).
129. J. F. Qian, Y. Xiong, Y. L. Cao, X. P. Ai, and H. X. Yang, "Synergistic Na-Storage Reactions in Sn_4P_3 as a High-Capacity, Cycle-stable Anode of Na-Ion Batteries," *Nano Lett.*, **14** [4] 1865-69 (2014).